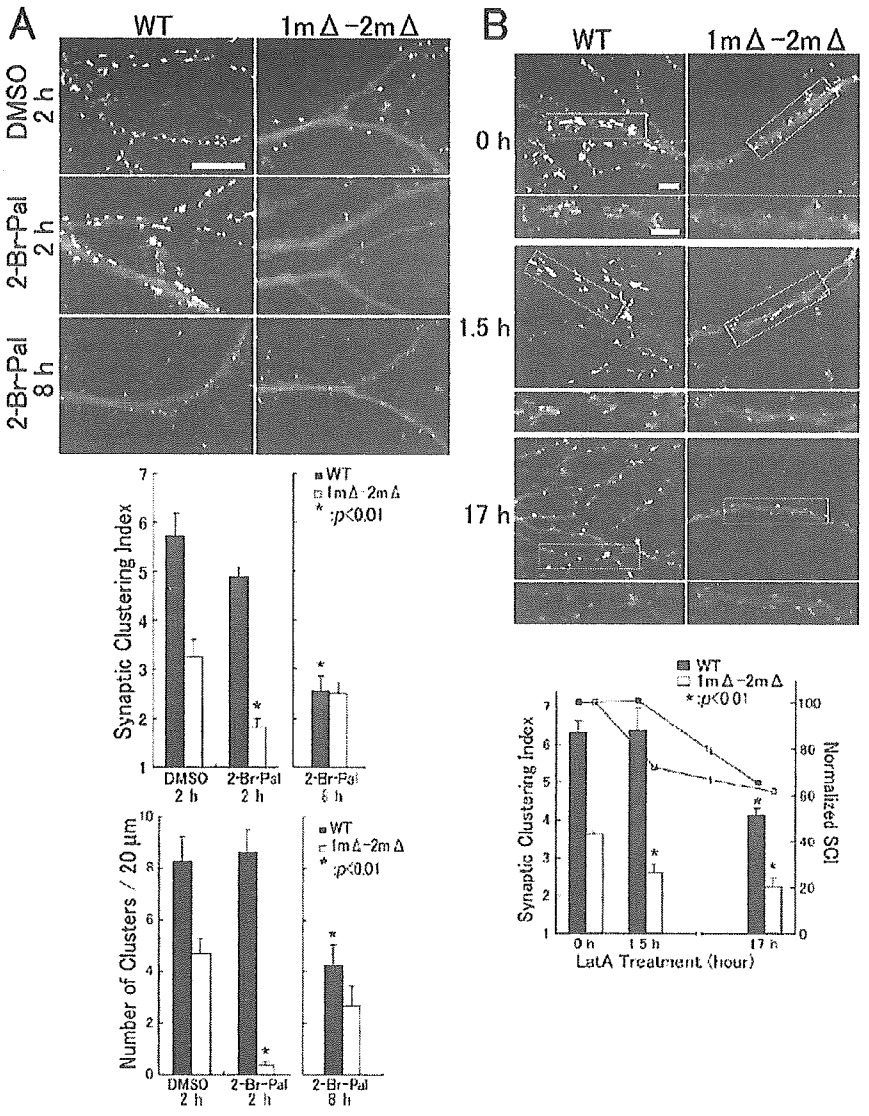

Figure 6. Ligand-binding-deficient mutants are more loosely anchored to the postsynaptic membrane than the wild type. ***A***, Synaptic clusters in neurons expressing ligand-binding-deficient PSD-95 mutants are rapidly dispersed in response to treatment with a palmitoylation blocker, 2-Br-Pal. 2-Br-Pal dramatically reduces the clustering efficiencies in neurons expressing the mutant PSD-95 (1mΔ–2mΔ–N326S) but only moderately in neurons expressing the wild-type PSD-95. Grayscale images show the PSD-95–GFP fluorescence of the wild-type and 1mΔ–2mΔ-expressing neurons treated with DMSO or 2-Br-Pal for 2 or 8 h. The top graph summarizes the results of the SCI analysis of the DMSO-treated or 100 μM 2-Br-Pal-treated wild-type and 1mΔ–2mΔ-expressing neurons. The bottom graph shows the cluster density (number of clusters per 20 μm dendritic segment) of the same datasets. $*p < 0.01$ versus the SCI of DMSO 2 h by the Student's *t* test. ***B***, Increased susceptibility to an actin-depolymerizing drug (LatA) in neurons expressing a ligand-binding-deficient mutant. Actin depolymerization by 5 μM latrunculin A caused much faster cluster dissociation in the 1mΔ–2mΔ mutant PSD-95-expressing neurons. Grayscale images of the wild-type and 1mΔ–2mΔ-expressing neurons treated with LatA for 0, 1.5, and 17 h. The small images below are the colored images (PSD-95–GFP, green) merged with synaptophysin staining (red) of the areas outlined by the white rectangles in the grayscale images. The graph shows the SCI values of the LatA-treated and nontreated wild-type and 1mΔ–2mΔ-expressing neurons. Raw values are shown as bar graphs (left *y*-axis), and scaled values (normalized to SCI at 0 h) are shown as line graphs (right *y*-axis). $*p < 0.01$ versus the SCI of nontreated (0 h) WT and 1mΔ–2mΔ, respectively, by the Student's *t* test. Scale bars, 10 μm.

previous experiments using 2-bromo-palmitate treatments, the mutant (1mΔ–2mΔ) PSD-95, during actin depolymerization, seemed to be more likely than the wild type to move away from synaptic clusters, although the presynaptic marker staining remained intact. Thus, the PDZ1/2 binding activity probably plays a critical role in facilitating postsynaptic clustering, in conjunction with a postsynaptic actin polymerization-dependent process.

Together, these data demonstrated that the clusters containing PDZ-binding-deficient PSD-95 mutants were more sensitive to treatment with a palmitoylation inhibitor or an actin depolymerization reagent. These results are consistent with the idea that efficient PDZ-ligand binding strongly promotes the clustering of PSD-95 and stabilizes the membrane anchoring, subsequent to a step after the activity-dependent palmitate cycling and the actin cytoskeleton-dependent attachment of the PSD-95 to the PSD complex.

These experiments alone may not formally rule out the possibility that the apparently increased susceptibility of the 1mΔ–2mΔ mutant-containing clusters to disperse during various manipulations (treatments with either a palmitoylation inhibitor or an actin depolymerization reagent) might be at least partially elicited by subtle reductions in the absolute amounts of expressed proteins in various local dendritic compartments rather than by a decrease in PDZ-ligand binding. We do not favor this interpretation, however, because the low expression level of wild-type PSD-95–GFP (less than the cutoff threshold of 100; see Materials and Methods) was not accompanied by a reduction in the SCI (data not shown).

To obtain independent support for the PDZ-ligand-binding-mediated stabilization of the localization of PSD-95 to the PSD, we performed additional quantitative measurements of PSD alterations, including spine morphology.

The PDZ-ligand-binding deficiency is correlated with a severe defect in the dendritic localization of PSD-95 clusters and may affect spine morphology

Consistent with the suggestion that the stability of PSD-95 may be compromised at postsynaptic clusters expressing PDZ-ligand-binding mutants, the overexpression of PSD-95–GFP with dysfunctional PDZ domains generated a significantly large number of synaptic clusters that were located away from the parent dendritic shaft (Figs. 3*D*,*H*,*J*, insets, 7*A*, 8) ($p < 0.001$, Kolmogorov–Smirnov test). In contrast, the wild-type PSD-95 clusters were formed directly on the dendritic shaft (Figs. 3*A*, 7*A*, 8), consistent with previous reports. To quantify this phenotype, we reanalyzed the same dataset of cells shown in Figures 3 and 4, measured the projected distance between each synaptic cluster and the closest dendritic shaft (cluster-shaft distance; when clusters were formed within the boundary of the dendritic shaft in a maximal projection image, the distance was considered as zero), and compared this index among the various types of mutants (Fig. 7*A*).

Most of the wild-type PSD-95 clusters were formed directly on

the dendrite (80.7% of the clusters were shaft clusters), and the average ± SEM apparent distance was 0.18 ± 0.029 μm, within the limit of the optical spatial resolution. Untransfected neurons analyzed with the anti-PSD-95 antibody staining produced a qualitatively similar value (0.10 ± 0.030 μm vs WT; $p > 0.05$, Kolmogorov–Smirnov test; data not shown), again within the limit of spatial resolution. In contrast, the average cluster-shaft distance of 1mΔ–2mΔ was significantly increased, to 0.47 ± 0.093 μm. In these 1mΔ–2mΔ expressing neurons, the cluster-shaft distance values showed a non-Gaussian distribution, which was quite distinct from that of the wild-type expressing neurons ($p < 0.001$, Kolmogorov–Smirnov test), with >40% of the clusters being significantly distant (this distance ranged from 0.2 to 3 μm) from the nearest shaft (Figs. 7*A*, 8). The clusters that formed far from dendrites did not form on immature filopodia/spines, because they were all juxtaposed with presynaptic markers, such as synaptophysin and VGLUT1 (Fig. 2). Thus, the formation and attraction of presynaptic boutons to the sites of PSD-95 clusters were not impaired at all, even in the PSD-95 mutant expressing neurons.

We wondered whether the PDZ-ligand-binding affinity might regulate this distance between the PSD-95 cluster and the shaft. To examine this possibility, we measured the cluster-shaft distance in all of the available PSD-95 mutants. Single PDZ mutants (1mΔ–2 or 1–2mΔ) had fewer shaft clusters (69.3 and 73.2%, respectively) compared with the wild type, and, in these cells, many clusters were found on the heads of spine-like protrusions. Similarly, in the PDZ3 N326S mutant expressing neurons, some of the clusters were formed on the spines, whereas 70.7% of the clusters were on the shafts (Fig. 8). The severest phenotype was found in the 1mΔ–2mΔ–N326S mutant expressing neurons, which had only 43.8% of the shaft clusters. Some of these were farther from the dendritic shafts and seemed to form on the cross-sections of thin, long protrusions from the dendrites.

Together, these data indicated that the average cluster-shaft distance was qualitatively (Fig. 3) and quantitatively (Figs. 7*A*, 8) longer in the mutant type with a lower SCI value. In fact, a statistically significant negative correlation was found between the SCI and the cluster-shaft distance (the coefficient of correlation, $r = -0.8637$; $p < 0.01$) (Fig. 7*B*).

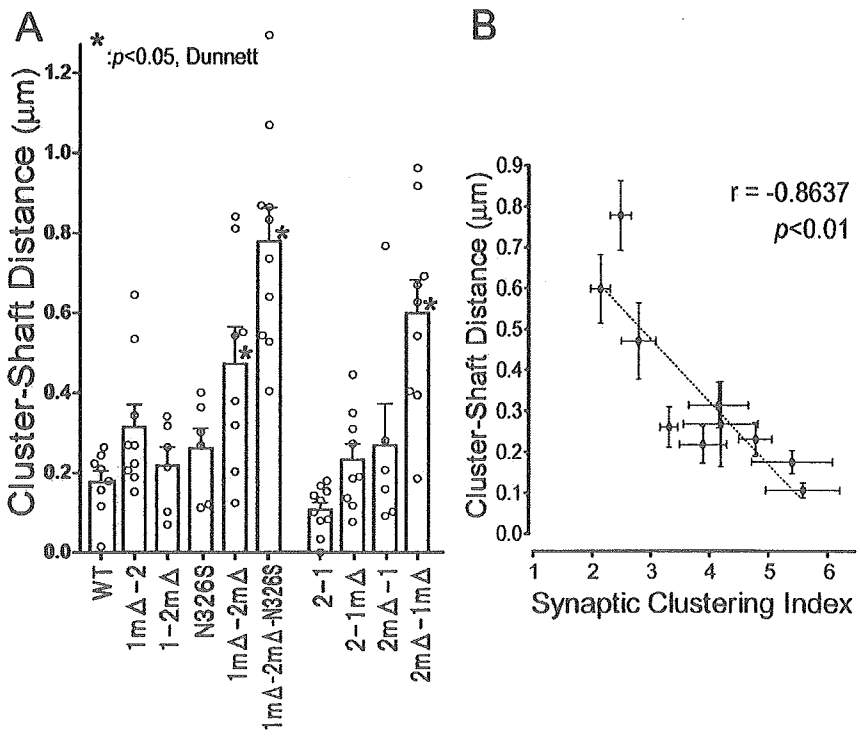

Figure 7. The cluster-shaft distance is increased in the mutant-expressing neurons compared with the wild-type-expressing neurons and negatively correlates with the SCI value. *A*, Ligand-binding-deficient PSD-95 mutants formed clusters on tips of protrusions (spines) away from the dendritic shafts. The distance from the center of the synaptic clusters to the edge of the parent dendritic shaft was measured on the same dataset of cells used to calculate the SCI (Figs. 3, 4). To the shaft clusters (clusters that appeared to be formed directly on the dendritic shaft), the value 0 was arbitrarily assigned. Bars and error bars represent the averages and the SEMs of the calculated means of each cell (open dots). The error bars of WT and 2–1 are exceptionally small, because these cells predominantly have shaft clusters to which we applied the same values equally, and the large fraction of the shaft clusters will result in average distances below 0.2 μm. *$p < 0.05$ versus WT. *B*, The SCI is negatively correlated with the cluster-shaft distance. The average SCI and the average cluster-shaft distance, the distance from the PSD-95 clusters to the dendritic shaft, of the wild type and each mutant type ($n = 6–10$ cells per mutant type), are plotted on the *x*-axis and *y*-axis, respectively. Error bars indicate SEM. The broken line shows the fitted regression line ($r = -0.8637$; $p < 0.01$).

The loss of PDZ binding in synGAP replicates the clustering and morphological phenotypes of PDZ-ligand-binding-deficient PSD-95

One candidate PDZ ligand that may be involved in the phenotypes associated with the overexpression of mutant PSD-95 is synGAP (Fig. 5). To directly test whether synGAP binding to PSD-95 is required for the efficient PSD-95 clustering and mature spine formation, we next examined the effects of overexpressing a synGAP C-terminal deletion mutant with diminished binding ability to the PDZ domains [synGAP(ΔSXV)]. We cotransfected the wild-type synGAP(TRV) with the intact C-terminal PDZ-binding motif or the mutant synGAP(ΔSXV), which lacks five C-terminal residues, QQTRV (Vazquez et al., 2004), together with the wild-type PSD-95–GFP. The expression of the synGAP(ΔSXV) caused the PSD-95(WT)–GFP to become distributed in an aberrant pattern with a reduced SCI, very similar to that of the ligand-binding-deficient PSD-95, i.e., 1mΔ–2mΔ (Fig. 9*A*,*B*). The localization of synGAP(ΔSXV) no longer overlapped with that of PSD-95, although many nonsynaptic synGAP clusters were detectable (Fig. 9*A*), presumably because of interactions with proteins other than PSD-95 (Tomoda et al., 2004). In contrast, the expression of the wild-type synGAP(TRV) did not change the pattern of PSD-95 localization, and the synGAP(TRV) colocalized well with the PSD-95 clusters (Fig. 9*A*,*B*). Similarly, the defect in synaptic clustering and the increase in cluster-shaft distance found in neurons expressing the 1mΔ–2mΔ mutant (Figs. 4, 7) were primarily replicated by the coexpression of PSD-95(WT)–GFP with the synGAP(ΔSXV) mutant (Fig. 9*C*,*D*). Consistently, the cluster density (the number of clusters per 20 μm dendritic segment) was greatly reduced in parallel (Fig. 9*C*), and, conversely, the cluster-shaft distance was elongated (Fig. 9*D*). This effect was specific for the PDZ-binding motif mutant synGAP(ΔSXV) and was not found with a mutant

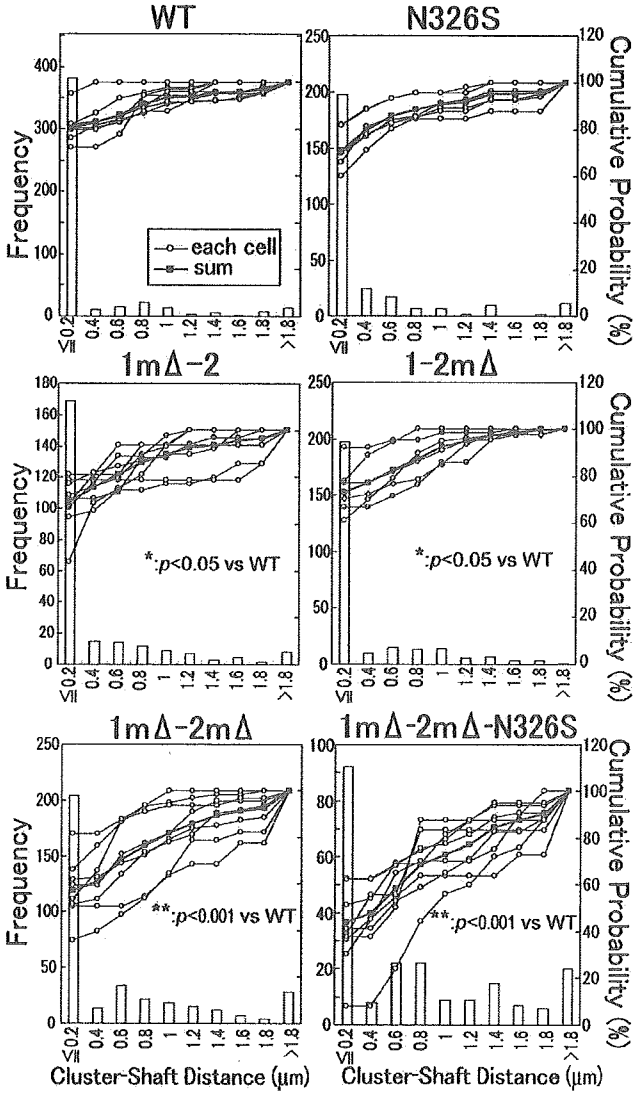

Figure 8. Histograms of the cluster-shaft distance distributions in the PSD-95 wild-type- and mutant-expressing neurons. The cumulative probability (right *y*-axis) of the cluster distances for each individual cell is traced (lines with open circles), and the aggregate data are traced (thicker lines with filled squares). The frequency histogram of the aggregate data were superimposed (left *y*-axis). Note that, in the mutant-expressing neurons, the cluster-shaft distance distribution cannot be fitted with a single Gaussian distribution, because they have a substantial portion of nonshaft clusters. This discrepancy is statistically significant. $*p < 0.05$ and $**p < 0.001$ versus WT by Kolmogorov–Smirnov test.

synGAP lacking GAP activity synGAP(GAP*) (data not shown). These data are consistent with the notion that the interaction of synGAP with the PDZ domains of PSD-95 may be essential for the efficient cluster formation at a higher density along the dendrites and the proper localization of the PSD-95 clusters closer to the dendritic shafts.

Additionally, we noticed that the combined expression of the 1mΔ–2mΔ mutant of PSD-95 and the synGAP(ΔSXV) mutant enhanced the phenotypes (reduced SCI, diminished synaptic clusters, and larger cluster-shaft distances) compared with neurons coexpressing the PSD-95(WT)–GFP in the presence of the synGAP(ΔSXV) mutant (Fig. 9*B–D*). Thus, primary PDZ ligands of PSD-95 distinct from synGAP may also contribute to the synaptic clustering and morphological phenotypes associated with decreased PDZ binding.

These findings together raise the possibility that the PDZ-ligand binding of PSD-95, in part via synGAP, may play a direct role in the synaptic clustering of PSD-95, while also directing the localization of PSD-95 containing clusters toward the vicinity of the dendritic shafts, perhaps during the final step of spine maturation.

Discussion

The localization and function of many essential synaptic proteins are regulated by molecular interactions with PDZ-containing scaffolding proteins. However, the molecular mechanisms that regulate the clustering of such PSD scaffolds at synapses are not fully understood. In this report, PDZ-ligand-binding-deficient, full-length PSD-95 mutants were used to probe the contribution of each of the three PDZ-ligand-binding affinities in various aspects of PSD-95-mediated PSD organization.

Independent and additive contributions of each PDZ domain to PSD-95 clustering and recruiting PDZ ligands to the PSD scaffold

Previous studies showed that at least one PDZ domain was needed to target the PSD-95 to the synapse, in addition to the requirement of the N-terminal region including the palmitoylated pair of cysteines, which is essential for multimerization and membrane targeting (Craven et al., 1999; Hsueh and Sheng, 1999; Christopherson et al., 2003). Furthermore, the inhibition of the PDZ3 binding to the microtubule-binding protein CRIPT impaired the synaptic clustering of the PSD-95 (Passafaro et al., 1999). We also found that overexpression of a ligand-binding-deficient PDZ3 mutant of PSD-95 with a single point mutation, in cultured hippocampal neurons, significantly reduced the clustering efficiency of PSD-95 at synapses. This indicated that the interaction between the PDZ3 and its ligand(s) plays an important role in clustering PSD-95 at the synapses. Importantly, by extending the mutagenesis to the ligand-binding sites of PDZ1 and PDZ2, we demonstrated that the ligand-binding activities of PDZ1 and PDZ2 were equally critical for the efficient clustering of PSD-95. Furthermore, the impact of losing the PDZ-binding affinities one by one accumulated in an approximately additive manner. Thus, our data indicated that each individual binding event at each PDZ domain of PSD-95 independently and approximately additively contributes to the additional clustering of PSD-95 at the synapses.

We further verified this conclusion by a mutant study using one of the major ligand proteins, synGAP. The absence of the PDZ-binding motif of synGAP produced a pattern of results quite similar to those obtained with the ligand-binding-deficient PSD-95 mutants and strongly affected both the PSD-95 clustering and the spine morphology. In keeping with the results obtained by a systematic introduction of the mutations to the PDZ domains, the synGAP mutant data suggested that the presence of PSD-95 ligand-binding motifs is not sufficient, but rather an intact synGAP-PSD-95 interaction, mediated via PDZ-binding, is necessary for the clustering and the functions of PSD-95.

Our results also revealed that the ligand-binding-deficient mutants exhibited significantly weaker associations with the PSD. The 2-bromo-palmitate treatment easily dispersed the mutant PSD-95–GFP molecules from their clusters. These results support the notion that PSD-95 is anchored to the PSD by both the palmitate modification and the ligand-PDZ domain interactions. Furthermore, the clusters expressing PSD-95 mutants became extremely labile after F-actin depolymerization by the LatA treatment, consistent with the possibility that the mutant PSD-95

was unable to reach the core fraction of the PSD and thus became mislocalized toward the peripheral, cytoskeleton-dependent fraction of the PSD (Allison et al., 2000; Zhang and Benson, 2001). Together, the data suggested that the tight and stable association of PSD-95 with the PSD requires the interactions of the PDZ domains with their ligands, as well as the appropriate PSD-95 lipidification and actin polymerization.

Our results also suggested that each ligand-binding event at the PDZ domains may additionally fulfill two other separate functions in parallel: efficient targeting of PSD-95 to the spines, and stable recruitment and incorporation of PSD-95 ligands into the PSD. In this regard, it may be useful to consider two distinct classes of PSD-95 ligands: one class including PSD-95-specific ligands, such as synGAP, and another class that includes scaffold-independent ligands, such as NMDA receptor subunits, which, for example, can tightly interact with synapse-associated protein 102 (SAP102) as well. Although the latter may still become localized to the synapses in the absence of PSD-95 (Migaud et al., 1998; Rao et al., 1998), our data suggested that PDZ-ligand binding strongly contributes to the tight association of these two classes of proteins as stable multiprotein networks in the vicinity of synapses.

Another implication of our work, in view of the approximately additive effect of the three PDZ domains in the clustering of PSD-95, is that the tightness of the PSD association with the PSD protein complex may be tuned and controlled as a function of the number of PDZ-ligand-binding events. The intermolecular MAGUK interaction is reportedly activity regulated, at least in the case of SAP97 (Nakagawa et al., 2004). Whether this activity dependence in MAGUK clustering and dispersion is actually mediated by the PDZ-ligand binding still remains to be demonstrated. If this is the case, then the clustering efficiency of the MAGUK-like scaffolds, such as PSD-95, could be dynamically modulated depending on the local synaptic activity, thereby accounting for the requirement for multivalent scaffolding proteins in the regulation of synaptic plasticity (Migaud et al., 1998; Ehrlich and Malinow, 2004; Nakagawa et al., 2004).

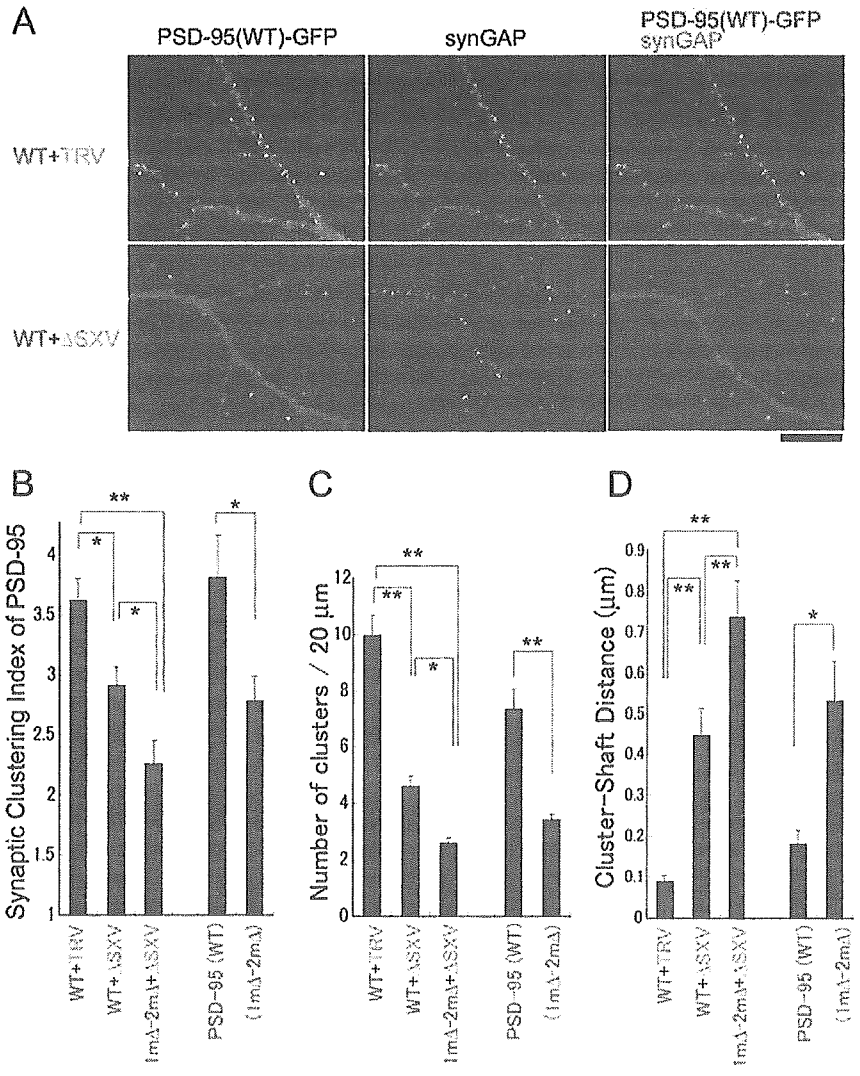

Figure 9. Overexpression of a mutant synGAP lacking the C-terminal PDZ-binding motif results in a severe defect in the PSD-95 cluster formation and a significant increase in the PSD-95 cluster-shaft distance. ***A***, Immunolocalization of PSD-95 clusters [PSD-95(WT)–GFP] and synGAP in neurons coexpressing the wild-type PSD-95 and either the wild-type synGAP (TRV, top panels) or the PDZ-binding motif mutant synGAP (ΔSXV, bottom panels). Neurons were cotransfected at 8 DIV and fixed at 10 DIV. The coexpression of wild-type synGAP(TRV) with wild-type PSD-95 did not result in a detectable change in the clustering efficiency and cluster density compared with the overexpression of PSD-95(WT)–GFP alone. Remarkably, during coexpression with synGAP(ΔSXV), PSD-95(WT)–GFP displayed an aberrant dendritic distribution that was similar to the phenotypes seen with the ligand-binding-deficient PSD-95 mutant (i.e., 1mΔ–2mΔ). ***B–D***, Quantification of the defects seen in synaptic cluster formation and in spine morphology. Based on the images of PSD-95–GFP, the SCI values (***B***), the cluster density (the number of synaptic clusters per 20 μm dendritic segment) (***C***), and the cluster-shaft distance (***D***) were measured in the neurons expressing the indicated constructs and are shown as bar graphs. We confirmed that the PSD-95 clusters analyzed were all juxtaposed to the synaptophysin-staining puncta. Scale bar, 10 μm. $^*p < 0.05$, $^{**}p < 0.01$, by one-way ANOVA with *post hoc* Tukey's test (n = 12–16 neurons); or $^*p < 0.05$, $^{**}p < 0.01$, by the Student's t test in the experimental pairs of PSD-95(WT)–GFP only and PSD-95(1mΔ–2mΔ)–GFP only.

Possible recruitment of a morphogenic signaling complex via PSD-95 during synapse development

In our hands, the ligand-binding-deficient PSD-95 not only reduced the clustering efficiency and altered the composition of the PSD but also localized its own clusters far from the dendritic shafts in hippocampal neurons (Figs. 3, 7). The aberrant PSD cluster location and the higher frequency of elongated spine morphology were consistently observed in both a transient plasmid expression protocol by gene delivery at 8–9 DIV and after a long-term expression protocol by electroporation at 0 DIV, with subsequent 12–13 d cultures. Because no gross morphological change was reported in the PSD-95 knock-out mouse (Migaud et al., 1998), it may appear, at first glance, that the defect in the PSD cluster localization seen in our culture could be interpreted as an experimental artifact. However, we believe that this is not the case for two reasons. First, the PSD location and the spine morphol-

ogy defects are not observed in all spines but only in a minority of the spines within a mutant PSD-95 expressing neuron (at most, 20.8% of spines longer than 1 μm, even in the severest case). Therefore, a large-scale quantification study in the knock-out mice brain, using serial electron microscopy over entire dendritic trees, would be needed to corroborate our findings, but such an effort was not undertaken in the initial screen (Migaud et al., 1998). Second, we observed correlations not only between the synaptic clustering index and the cluster-shaft distance (a negative correlation) but also between the PSD-95 cluster formation and the synGAP recruitment (a positive correlation). Indeed, synGAP, a GTPase-activating protein for Ras, was less densely localized at postsynaptic sites in the 1mΔ–2mΔ–N326S expressing neurons, whereas Shank/Synamon, Homer 1c/Ves1-L/PSD-Zip45, and PSD-93/Chapsin-110 were normally localized, as in the wild-type PSD-95 expressing neurons. Most critically, a synGAP mutant lacking the C-terminal PDZ-binding motif showed effects similar to those seen with PSD-95 mutants. These results are consistent with the idea that synGAP, in part downstream of PSD-95, may function in the clustering and movement of the PSD proteins in the spines. Furthermore, synGAP reportedly also negatively regulates spine formation and limits spine head expansion and filopodial extension (Vazquez et al., 2004). Together, alterations in the distribution and the PSD clustering of synGAP may at least partially account for the aberrant phenotype observed in cultured neurons. Thus, PSD-95 may play a role in recruiting a morphogenic signaling complex within the PSD complex.

Such a view is consistent with the following experimental results. (1) The morphological changes associated with the wild-type PSD-95 overexpression were shown to increase both the number and size of the spines, together with the accelerated synaptic maturation (El-Husseini et al., 2000). (2) Several partners interacting with PSD-95, such as Citron (Furuyashiki et al., 1999), CRIPT (Niethammer et al., 1998), and SPAR (spine-associated RapGAP) (Pak et al., 2001), were shown to interact with cytoskeletal elements. The overexpression of related scaffold proteins, such as Homer and Shank, which closely interact with actin cytoskeletal components (Naisbitt et al., 1999; Shiraishi et al., 1999), reportedly induces spine head enlargement (Sala et al., 2001). (3) A growing list of morphogenic signaling molecules has been identified within the PSD complex, such as FMR1 (the fragile X mental retardation gene) (Comery et al., 1997; Nimchinsky et al., 2001), LIM kinase (Meng et al., 2002), N-cadherin (Togashi et al., 2002), ephrinA3-EphA4 (Murai et al., 2003), cortactin (Hering and Sheng, 2003), Rho-GEF (guanine nucleotide exchange factor) Kalirin-7 (Penzes et al., 2001), and EphB2 (Murai et al., 2003). Because PSD-95-ligand binding is critical for maintaining proper PSD organization, impairments of the scaffolding functions of PSD-95 might indirectly disrupt the PSD localization and the spine maturation by triggering the misorchestration of a morphogenic signaling complex.

In summary, this work demonstrates that the ligand-binding activities of each of the three PDZ domains are essential for PSD-95 to organize the PSD properly and are likely to be involved in achieving normal spine development, in part via interactions with synGAP. We found that the multivalent binding nature of PSD-95 plays a key role in the dynamic regulation of PSD protein clustering. Our study thus provides new insights into the structural basis of the role of PSD-95 in synaptic development and plasticity.

References

Allison DW, Gelfand VI, Spector I, Craig AM (1998) Role of actin in anchoring postsynaptic receptors in cultured hippocampal neurons: differential attachment of NMDA versus AMPA receptors. J Neurosci 18:2423–2436.

Allison DW, Chervin AS, Gelfand VI, Craig AM (2000) Postsynaptic scaffolds of excitatory and inhibitory synapses in hippocampal neurons: maintenance of core components independent of actin filaments and microtubules. J Neurosci 20:4545–4554.

Arnold DB, Clapham DE (1999) Molecular determinants for subcellular localization of PSD-95 with an interacting K^+ channel. Neuron 23:149–157.

Brenman JE, Topinka JR, Cooper EC, McGee AW, Rosen J, Milroy T, Ralston HJ, Bredt DS (1998) Localization of postsynaptic density-93 to dendritic microtubules and interaction with microtubule-associated protein 1A. J Neurosci 18:8805–8813.

Chen HJ, Rojas-Soto M, Oguni A, Kennedy MB (1998) A synaptic Ras-GTPase activating protein (p135 SynGAP) inhibited by CaM kinase II. Neuron 20:895–904.

Cho KO, Hunt CA, Kennedy MB (1992) The rat brain postsynaptic density fraction contains a homolog of the *Drosophila* discs-large tumor suppressor protein. Neuron 9:929–942.

Christopherson KS, Sweeney NT, Craven SE, Kang R, El-Husseini Ael D, Bredt DS (2003) Lipid- and protein-mediated multimerization of PSD-95: implications for receptor clustering and assembly of synaptic protein networks. J Cell Sci 116:3213–3219.

Comery TA, Harris JB, Willems PJ, Oostra BA, Irwin SA, Weiler IJ, Greenough WT (1997) Abnormal dendritic spines in fragile X knockout mice: maturation and pruning deficits. Proc Natl Acad Sci USA 94:5401–5404.

Craven SE, El-Husseini AE, Bredt DS (1999) Synaptic targeting of the postsynaptic density protein PSD-95 mediated by lipid and protein motifs. Neuron 22:497–509.

Ehrlich I, Malinow R (2004) Postsynaptic density 95 controls AMPA receptor incorporation during long-term potentiation and experience-driven synaptic plasticity. J Neurosci 24:916–927.

El-Husseini AE, Schnell E, Chetkovich DM, Nicoll RA, Bredt DS (2000) PSD-95 involvement in maturation of excitatory synapses. Science 290:1364–1368.

El-Husseini Ael D, Schnell E, Dakoji S, Sweeney N, Zhou Q, Prange O, Gauthier-Campbell C, Aguilera-Moreno A, Nicoll RA, Bredt DS (2002) Synaptic strength regulated by palmitate cycling on PSD-95. Cell 108:849–863.

Furuyashiki T, Fujisawa K, Fujita A, Madaule P, Uchino S, Mishina M, Bito H, Narumiya S (1999) Citron, a Rho-target, interacts with PSD-95/SAP-90 at glutamatergic synapses in the thalamus. J Neurosci 19:109–118.

Furuyashiki T, Arakawa Y, Takemoto-Kimura S, Bito H, Narumiya S (2002) Multiple spatiotemporal modes of actin reorganization by NMDA receptors and voltage-gated Ca^{2+} channels. Proc Natl Acad Sci USA 99:14458–14463.

Hammer O, Harper DAT, Ryan PD (2001) PAST: paleontological statistics software package for education and data analysis. Palaeontologia Electronica 4:9.

Hering H, Sheng M (2003) Activity-dependent redistribution and essential role of cortactin in dendritic spine morphogenesis. J Neurosci 23:11759–11769.

Hsueh YP, Sheng M (1999) Requirement of N-terminal cysteines of PSD-95 for PSD-95 multimerization and ternary complex formation, but not for binding to potassium channel Kv1.4. J Biol Chem 274:532–536.

Imamura F, Maeda S, Doi T, Fujiyoshi Y (2002) Ligand binding of the second PDZ domain regulates clustering of PSD-95 with the Kv1.4 potassium channel. J Biol Chem 277:3640–3646.

Irie K, Nakatsu T, Mitsuoka K, Miyazawa A, Sobue K, Hiroaki Y, Doi T, Fujiyoshi Y, Kato H (2002) Crystal structure of the Homer 1 family conserved region reveals the interaction between the EVH1 domain and own proline-rich motif. J Mol Biol 318:1117–1126.

Irie M, Hata Y, Takeuchi M, Ichtchenko K, Toyoda A, Hirao K, Takai Y, Rosahl TW, Sudhof TC (1997) Binding of neuroligins to PSD-95. Science 277:1511–1515.

Kim E, Niethammer M, Rothschild A, Jan YN, Sheng M (1995) Clustering of Shaker-type K^+ channels by interaction with a family of membrane-associated guanylate kinases. Nature 378:85–88.

Kim JH, Liao D, Lau LF, Huganir RL (1998) SynGAP: a synaptic RasGAP that associates with the PSD-95/SAP90 protein family. Neuron 20:683–691.

Kornau HC, Schenker LT, Kennedy MB, Seeburg PH (1995) Domain interaction between NMDA receptor subunits and the postsynaptic density protein PSD-95. Science 269:1737–1740.

Long JF, Tochio H, Wang P, Fan JS, Sala C, Niethammer M, Sheng M, Zhang M (2003) Supramodular structure and synergistic target binding of the N-terminal tandem PDZ domains of PSD-95. J Mol Biol 327:203–214.

McGee AW, Dakoji SR, Olsen O, Bredt DS, Lim WA, Prehoda KE (2001) Structure of the SH3-guanylate kinase module from PSD-95 suggests a mechanism for regulated assembly of MAGUK scaffolding proteins. Mol Cell 8:1291–1301.

Meng Y, Zhang Y, Tregoubov V, Janus C, Cruz L, Jackson M, Lu WY, MacDonald JF, Wang JY, Falls DL, Jia Z (2002) Abnormal spine morphology and enhanced LTP in LIMK-1 knockout mice. Neuron 35:121–133.

Migaud M, Charlesworth P, Dempster M, Webster LC, Watabe AM, Makhinson M, He Y, Ramsay MF, Morris RG, Morrison JH, O'Dell TJ, Grant SG (1998) Enhanced long-term potentiation and impaired learning in mice with mutant postsynaptic density-95 protein. Nature 396:433–439.

Murai KK, Nguyen LN, Irie F, Yamaguchi Y, Pasquale EB (2003) Control of hippocampal dendritic spine morphology through ephrin-A3/EphA4 signaling. Nat Neurosci 6:153–160.

Naisbitt S, Kim E, Tu JC, Xiao B, Sala C, Valtschanoff J, Weinberg RJ, Worley PF, Sheng M (1999) Shank, a novel family of postsynaptic density proteins that binds to the NMDA receptor/PSD-95/GKAP complex and cortactin. Neuron 23:569–582.

Nakagawa T, Futai K, Lashuel HA, Lo I, Okamoto K, Walz T, Hayashi Y, Sheng M (2004) Quaternary structure, protein dynamics, and synaptic function of SAP97 controlled by L27 domain interactions. Neuron 44:453–467.

Niethammer M, Valtschanoff JG, Kapoor TM, Allison DW, Weinberg TM, Craig AM, Sheng M (1998) CRIPT, a novel postsynaptic protein that binds to the third PDZ domain of PSD-95/SAP90. Neuron 20:693–707.

Nimchinsky EA, Oberlander AM, Svoboda K (2001) Abnormal development of dendritic spines in FMR1 knock-out mice. J Neurosci 21:5139–5146.

Okabe S, Kim HD, Miwa A, Kuriu T, Okado H (1999) Continual remodeling of postsynaptic density and its regulation by synaptic activity. Nat Neurosci 2:804–811.

Pak DT, Yang S, Rudolph-Correia S, Kim E, Sheng M (2001) Regulation of dendritic spine morphology by SPAR, a PSD-95-associated RapGAP. Neuron 31:289–303.

Passafaro M, Sala C, Niethammer M, Sheng M (1999) Microtubule binding by CRIPT and its potential role in the synaptic clustering of PSD-95. Nat Neurosci 2:1063–1069.

Penzes P, Johnson RC, Sattler R, Zhang X, Huganir RL, Kambampati V, Mains RE, Eipper BA (2001) The neuronal Rho-GEF Kalirin-7 interacts with PDZ domain-containing proteins and regulates dendritic morphogenesis. Neuron 29:229–242.

Petersen JD, Chen X, Vinade L, Dosemeci A, Lisman JE, Reese TS (2003) Distribution of postsynaptic density (PSD)-95 and Ca^{2+}/calmodulin-dependent protein kinase II at the PSD. J Neurosci 23:11270–11278.

Rao A, Kim E, Sheng M, Craig AM (1998) Heterogeneity in the molecular composition of excitatory postsynaptic sites during development of hippocampal neurons in culture. J Neurosci 18:1217–1229.

Sala C, Piech V, Wilson NR, Passafaro M, Liu G, Sheng M (2001) Regulation of dendritic spine morphology and synaptic function by Shank and Homer. Neuron 31:115–130.

Sheng M, Sala C (2001) PDZ domains and the organization of supramolecular complexes. Annu Rev Neurosci 24:1–29.

Shiraishi Y, Mizutani A, Bito H, Fujisawa K, Narumiya S, Mikoshiba K, Furuichi T (1999) Cupidin, an isoform of Homer/Vesl, interacts with the actin cytoskeleton and activated rho family small GTPases and is expressed in developing mouse cerebellar granule cells. J Neurosci 19:8389–8400.

Sprengel R, Single FN (1999) Mice with genetically modified NMDA and AMPA receptors. Ann NY Acad Sci 868:494–501.

Takemoto-Kimura S, Terai H, Takamoto M, Ohmae S, Kikumura S, Segi E, Arakawa Y, Furuyashiki T, Narumiya S, Bito H (2003) Molecular cloning and characterization of CLICK-III/CaMKIgamma, a novel membrane-anchored neuronal Ca^{2+}/calmodulin-dependent protein kinase (CaMK). J Biol Chem 278:18597–18605.

Tavares GA, Panepucci EH, Brunger AT (2001) Structural characterization of the intramolecular interaction between the SH3 and guanylate kinase domains of PSD-95. Mol Cell 8:1313–1325.

Togashi H, Abe K, Mizoguchi A, Takaoka K, Chisaka O, Takeichi M (2002) Cadherin regulates dendritic spine morphogenesis. Neuron 35:77–89.

Tomoda T, Kim JH, Zhan C, Hatten ME (2004) Role of Unc51.1 and its binding partners in CNS axon outgrowth. Genes Dev 18:541–558.

Vazquez LE, Chen HJ, Sokolova I, Knuesel I, Kennedy MB (2004) SynGAP regulates spine formation. J Neurosci 24:8862–8872.

Zhang W, Benson DL (2001) Stages of synapse development defined by dependence on F-actin. J Neurosci 21:5169–5181.

European Journal of Neuroscience, Vol. 22, pp. 2985–2994, 2005

Bi-directional regulation of postsynaptic cortactin distribution by BDNF and NMDA receptor activity

Junko Iki,[1,5] Akihiro Inoue,[1] Haruhiko Bito[3,4] and Shigeo Okabe[1,2,4,5]
[1]Department of Cell Biology, School of Medicine, Tokyo Medical and Dental University, Bunkyo-ku, Tokyo, 113–8519, Japan
[2]Molecular Neurophysiology Group, Neuroscience Research Institute, National Institute of Advanced Industrial Science and Technology (AIST), Tsukuba, Ibaraki, 305–8566, Japan
[3]Department of Neurochemistry, the University of Tokyo Graduate School of Medicine, Bunkyo-ku, Tokyo 113–0033, Japan
[4]Solution Oriented Research for Science and Technology (SORST), Japan Science and Technology Agency (JST), Kawaguchi, 332–0012, Japan
[5]COE Program for Brain Integration and its Disorders, Tokyo Medical and Dental University, Bunkyo-ku, Tokyo, 113–8519, Japan

Keywords: BDNF, cytoskeleton, mouse, NMDA receptor, postsynaptic density

Abstract

Cortactin is an F-actin-associated protein which interacts with the postsynaptic scaffolding protein Shank at the SH3 domain and is localized within the dendritic spine in the mouse neuron. Green fluorescent protein (GFP)-based time-lapse imaging revealed cortactin redistribution from dendritic cytoplasm to postsynaptic sites by application of brain-derived neurotrophic factor (BDNF). This response was mediated by mitogen-activated protein (MAP) kinase activation and was dependent on the C-terminal SH3 domain. In contrast, activation of *N*-methyl-D-aspartate (NMDA) receptors induced loss of cortactin from postsynaptic sites. This NMDA-dependent redistribution was blocked by an Src family kinase inhibitor. Conversely, increasing Src family kinase activity induced cortactin phosphorylation and loss of cortactin from the postsynaptic sites. Finally, blocking of endogenous BDNF reduced the amount of cortactin at the postsynaptic sites and an NMDA receptor antagonist prevented this reduction. These results indicate the importance of counterbalance between BDNF and NMDA receptor-mediated signalling in the reorganization of the postsynaptic actin cytoskeleton during neuronal development.

Introduction

The development of postsynaptic specializations, including dendritic spines and postsynaptic density (PSD), is influenced by both cell-autonomous factors and external molecular cues. Among the external molecular cues, brain-derived neurotrophic factor (BDNF), a member of the neurotrophin family (Thoenen, 1995; Bibel & Barde, 2000), is of special interest, as this molecule regulates dendritic growth of neocortical pyramidal neurons through activation of trkB receptor tyrosine kinase (McAllister *et al.*, 1995; Horch & Katz, 2002) and is transferred from presynaptic sites to postsynaptic neurons (Kohara *et al.*, 2001), though the contribution of presynaptic trkB receptors may not be completely excluded (Manabe, 2002). Because BDNF synthesis and release are regulated by neuronal activity (Zafra *et al.*, 1990; Kohara *et al.*, 2001), BDNF may function as an activity-dependent morphogen for the postsynaptic development. Another possible regulator of postsynaptic development is presynaptically released glutamate. Among postsynaptic glutamate receptors, *N*-methyl-D-aspartate (NMDA) receptors are thought to be important in activity-dependent remodeling of synaptic organization (Li *et al.*, 1994), mainly because calcium influx through NMDA receptors activates a variety of postsynaptic kinases and phosphatases (Nakanishi, 1992). Indeed, neocortex-specific deletion of NMDA receptors results in abnormal dendritic structure in the somatosensory cortex (Iwasato *et al.*, 2000). How do BDNF and NMDA receptor activity ultimately change cytoplasmic organization just beneath the PSD? NMDA receptor activation reorganizes several postsynaptic molecules including actin (Halpain *et al.*, 1998; Furuyashiki *et al.*, 2002; Okamoto *et al.*, 2004) and calcium/calmodulin-dependent protein kinase II (Shen & Meyer, 1999). While α-amino-3-hydroxy-5-methyl-isoxazolepropionic acid (AMPA) receptor sorting has been linked to BDNF–trkB signalling in the developing thalamocortical synapses (Itami *et al.*, 2003), there have yet been few examples of BDNF-dependent reorganization of postsynaptic molecules. Furthermore, little is known about whether there exist any interactions between BDNF-dependent and NMDA receptor-dependent pathways for postsynaptic remodeling.

Actin plays a central role in the organization of submembraneous structure in many cellular systems. Actin filaments are highly concentrated within the dendritic spine, suggesting a key role in organization of the spine cytoplasm. In fact, recent experiments indicate multiple interactions between PSD scaffolding proteins and proteins involved in the actin cytoskeletal system (Wyszynski *et al.*, 1997; Allison *et al.*, 1998; Boeckers *et al.*, 1999). Among postsynaptic actin-associated proteins, cortactin has several unique properties. First, it interacts with both F-actin and the actin-related protein 2/3 complex (Du Weed *et al.*, 1998). Second, cortactin also binds to Shank, a PSD scaffolding protein (Naisbitt *et al.*, 1999). Third, cortactin is a substrate of the Src family tyrosine kinases including Fyn, which is

Correspondence: Dr Shigeo Okabe, [1]Department of Cell Biology, as above.
E-mail: okabe.cbio@tmd.ac.jp

Received 1 August 2005, revised 6 October 2005, accepted 7 October 2005

doi:10.1111/j.1460-9568.2005.04510.x

known to be involved in postsynaptic signalling pathways (Wu *et al.*, 1991; Wu & Parsons, 1993). Thus cortactin is well suited to couple postsynaptic signalling between the PSD and the actin cytoskeleton. Indeed, a previous study revealed NMDA receptor-dependent reduction of cortactin at the postsynaptic sites (Hering & Sheng, 2003). Here we show regulation of cortactin redistribution by BDNF and NMDA receptor activity during development of hippocampal neurons. Our results suggest the importance of counterbalance between BDNF and NMDA receptor activation in the development of the postsynaptic actin cytoskeleton.

Materials and methods

Generation of recombinant adenoviruses and hippocampal cultures

The generation and characterization of recombinant adenoviruses expressing PSD-95-enhanced green fluorescent protein (EGFP), PSD-95-enhanced yellow fluorescent protein (EYFP) and EGFP-actin have been described previously (Okabe *et al.*, 1999, 2001; Furuyashiki *et al.*, 2002). Mouse cortactin A, B and C cDNAs were cloned by PCR. Cortactin A, B and C, C-terminally labelled with enhanced cyan fluorescent protein (ECFP), were constructed by inserting full-length cDNA into pECFP-N1 (Clontech, Palo Alto, CA, USA). SH3 deletion construct (1–487) and triple phenylalanine mutation constructs (Y421F, Y466F and Y482F) were generated from Cortactin A cDNA using PCR and the QuickChange Site-Directed Mutagenesis kit (Strategene, La Jolla, CA, USA), respectively. Replication-deficient adenoviruses expressing cortactin A, B and C, and cortactin A mutants tagged with ECFP, were prepared as described previously (Okabe *et al.*, 1999). All animal experiments performed in this study have been carefully reviewed and approved by the Tokyo Medical and Dental University animal experiments committee (approval number: 0050274). Pregnant mice were briefly anaesthetized with ether, then killed by cervical dislocation. Preparation of hippocampal cultures from 17-day-old embryonic mice has been described previously (Okabe *et al.*, 1999). Cells were maintained for 10–23 days in culture and then exposed to adenoviruses at a multiplicity of infection of 20–60. Cells were observed by confocal microscopy after 24–48 h. Under this infection and observation protocol, the level of cortactin expression was 150–200% of the endogenous level and we did not observe any change in dendritic morphology and densities of PSD-95- or synaptophysin-immunoreactive puncta. For imaging, we assayed primary neurons expressing cortactin A and its mutants tagged with ECFP. For immunoprecipitation and immunoblotting, both cortactin A and B tagged with ECFP were characterized.

Immunocytochemistry and immunoblotting

Cells were fixed in 2% paraformaldehyde in PBS for 25 min at room temperature or with methanol for 10 min at −20 °C, permeabilized by incubating with 0.2% Triton X-100 in PBS for 5 min, blocked with 5% normal goat serum and incubated with mouse monoclonal anticortactin (Upstate Biotechnology, Lake placid, NY, USA), rabbit polyclonal anticortactin (Santa Cruz Biotechnology, Santa Cruz, CA, USA), mouse monoclonal anti-PSD-95 (Affinity Bioreagents, Golden, CO, USA), rabbit polyclonal anti-PSD-95 (Watanabe *et al.*, 1998), rabbit polyclonal anti-GKAP (a postsynaptic marker; Usui *et al.*, 2003), rabbit polyclonal anti-Shank (Usui *et al.*, 2003), rat polyclonal anti-Homer (Chemicon, Temecula, CA) and guinea pig polyclonal anti-VGLUT1 (a marker of excitatory presynaptic sites; Chemicon) antibodies. Primary antibodies were visualized with goat antimouse, antirabbit or antiguinea pig IgG conjugated to Cy3 (Jackson ImmunoResearch, West Grove, PA, USA) or Alexa 488 (Molecular Probes, Eugene, OR, USA). For the identification of the postsynaptic density, we utilized anti-PSD-95 and anti-Homer antibodies interchangeably. In mature neurons, the percentage of overlap in immunopositive clusters was >90%. A minor fraction of the culture preparation treated with H_2O_2 showed excitotoxicity. Therefore we fixed H_2O_2-treated cells with paraformaldehyde to check the absence of excitotoxicity and subsequently reacted them with rabbit anticortactin and rat anti-Homer. Anti-PSD-95 antibodies did not show specific staining when cells were fixed with paraformaldehyde. For H_2O_2 treatment, 20 neurons from two independent culture preparations were recorded and quantified for cluster density. For trkB–IgG treatment, 30 neurons from three independent culture preparations were analysed.

Immunoblotting was performed using rabbit polyclonal anti-GFP antibody (Molecular Probes) and mouse monoclonal antiphosphotyrosine antibody (Upstate Biotechnology). Primary hippocampal neurons infected with recombinant adenoviruses were extracted with RIPA buffer and immunoprecipitation was performed by using protein-G-conjugated agarose (Santa Cruz Biotechnology).

Pharmacological manipulation

Live cells were placed in a chamber containing Tyrode's solution [in mM: NaCl, 119; KCl, 2.5; Ca^{2+}, 2; Mg^{2+}, 2; 4-(2-hydroxyethyl)-1-piperazineethanesulphonic acid (HEPES), pH 7.4, 25; and glucose, 30) for 30 min before the experiment. The chamber was maintained at 37 °C by setting the temperature of the microscope stage to 37 °C, the microscope objective lens to 39 °C and the chamber lid to 40 °C. The concentrated stock of recombinant human BDNF, neurotrophin-3 (NT-3) and β-nerve growth factor (PeproTech EC, London, UK) in prewarmed Tyrode's solution was applied to the microscope chamber at final concentrations of 50 ng/mL. To evaluate the effects of protein kinase inhibitors, cells were incubated with each inhibitor for 15 min before application of BDNF at a concentrations of 200 nM for K252a (Alamone Laboratories, Jerusalem, Israel), 25 μM for 4-amino-5-(4-chlorophenyl)-7-(*t*-butyl)pyrazolo[3,4-*d*]pyrimidine (PP2; Calbiochem, Darmstadt, Germany), 10 μM for PD098059 (Biomol Research Laboratories, Plymouth Meeting, PA, USA) and 5 μM for LY294002 (Sigma, St Louis, MO, USA). We applied concentrated stock of jasplakinolide (Molecular Probes) in prewarmed Tyrode's solution to the chamber. The final concentration of jasplakinolide was 5 μM. To stimulate cells with NMDA, cells were pretreated with 10 μM 6-cyano-7-nitroquinoxaline-2,3-dione (CNQX; Tocris, Ballwin, MO, USA) and 2 μM tetrodeotoxin (TTX; Tocris) in Tyrode's solution for 15 min and subsequently exposed to 20 μM NMDA plus 10 μM CNQX and 2 μM TTX in Mg-free Tyrode's solution. The concentrated stock of H_2O_2 (10 mM) in Tyrode's solution was applied to culture medium in a final concentration of 100 μM. Hippocampal neurons in culture medium were exposed to trkB–IgG (R & D Systems, Minneapolis, MN, USA) at a concentration of 10 μg/mL for 5 days with or without D-(−)-2-amino-5-phosphonovaleric acid (APV; Tocris) at a concentration of 100 μM.

Microscopy and image analysis

Live cells were mounted in a chamber at 37 °C with a continuous flow of humidified 5% CO_2 to maintain the pH of the medium for long time-lapse experiments. In this configuration cells could be maintained without toxicity for >24 h. Alternatively, culture medium was replaced with Tyrode's solution and live cells were mounted in a

chamber at 37 °C without a continuous gas flow. Images were obtained on a Fluoview confocal laser-scanning microscope (Olympus, Melville, NY, USA). A 60× oil-immersion lens (NA 1.1) was used and images were collected at an additional electric zoom factor from 3× to 6×. For long time-lapse imaging, multiple optical sections (12–21 sections and *z*-spacing of 0.3–0.4 μm) were collected and these images were recombined using a maximum-brightness operation. To improve efficiency of time-lapse observation, multiple neurons (3–5 cells per experiment) on a cover slip separated by 100–500 μm from each other were imaged with intervals of 10–20 min automatically by using a macro program running on Fluoview software that regulates movements of both the *z*-axis step controller and the BIOST *x/y*-axis stage scanner (Sigma Koki, Tokyo Japan). Fluorescence recovery after photobleaching (FRAP) experiments were performed using a macro program to control sequential image acquisition and delivery of a photobleaching laser pulse to the region of interest defined by an acousto-optic tunable filter. Image analysis was performed using Metamorph software (Universal Imaging, West Chester, PA, USA) as previously described (Ebihara *et al.*, 2003). For a given time-lapse image series, all projection images were processed identically for cluster extraction and for quantitative analysis of fluorescence. For quantitative analysis of cluster intensity, segments of dendrites well separated from other structures were selected. Twenty to fifty clusters were measured for each time-lapse sequence and five independent experiments were analysed for individual pharmacological treatments. In each time-lapse experiment, image sequences of 3–5 neurons in multiple positions of the microscope stage were recorded. The total numbers of analysed neurons were in the range 9–16 for individual pharmacological treatments, because image sequences of several neurons were discarded mainly due to higher background fluorescence or larger fluctuations in the total fluorescence intensity. Control experiments were paired with individual pharmacological treatments and the data for control preparations were pooled if there was no statistical difference among groups. Therefore the total numbers of analysed neurons in control conditions were in the range 9–34.

Results

Dynamic properties of cortactin in hippocampal neurons

Recent immunohistochemical analysis has revealed concentration of cortactin in the dendritic spines (Racz & Weinberg, 2004). Consistent with this observation, immunocytochemical analysis of cortactin in cultured hippocampal neurons 3 weeks after plating showed extensive overlap of cortactin immunoreactivity with other PSD molecules including GKAP (Fig. 1A), PSD-95 and Homer (data not shown). Most cortactin-immunoreactive clusters were closely apposed to the structures immunopositive for VGLUT1, a marker of excitatory presynaptic sites. However, neurons at the early stage of development showed cortactin immunoreactivity within dendritic shafts where PSD proteins were absent. Thus cortactin shows gradual redistribution from nonsynaptic sites to the postsynaptic sites as neuronal maturation proceeds.

We generated ECFP-tagged cortactin (cortactin–ECFP) and expressed this fluorescent probe by using recombinant adenoviruses. In mature neurons, cortactin–ECFP was localized to the dendritic spines together with PSD-95–EYFP. Time-lapse imaging revealed persistent presence of cortactin clusters within spines for several hours (Fig. 1B). It has been shown that actin filaments within spines are highly dynamic and > 80% of actin molecules turn over within a few minutes (Star *et al.*, 2002). We confirmed this rapid turnover rate of actin in our culture preparation by using FRAP of EGFP–actin (data not shown). FRAP analysis of cortactin–ECFP revealed a 60% rapidly recovering fraction and a 40% stable fraction (Fig. 2). The presence of 40% stable cortactin indicates tight association of cortactin with the postsynaptic structure other than F-actin. Application of the actin-stabilizing reagent jasplakinolide did not alter the FRAP kinetics of cortactin, indicating that turnover of cortactin was not driven by actin depolymerization but was dependent on on–off rates of cortactin to the actin cytoskeleton.

Cortactin contains an N-terminal acidic domain functionally equivalent to the verprolin homology, cofilin homology and acidic domain of Wiskott–Aldrich syndrome protein (WASP) family proteins which activates actin polymerization by binding to the actin-related protein 2/3 complex (Martinez-Quiles *et al.*, 2004). The N-terminal acidic domain is followed by five or six tandem repeats of an actin-binding domain. The C-terminal SH3 domain of cortactin has been shown to interact with proline-rich sequences of a variety of proteins. Cortactin is also known as a substrate of the Src family kinases and phosphorylation can potentially regulate cortactin distribution (Selbach *et al.*, 2003). In mature hippocampal neurons, wild-type cortactin–ECFP accumulates in dendritic spines (Fig. 3) and the overall pattern of subcellular localization of two cortactin mutants, a triple phenylalanine mutant (Y421F, Y466F and Y482F) and an SH3-domain deletion mutant, was similar to the distribution of wild-type construct. The three tyrosine residues (Y421, Y466 and Y482) have been shown to be phosphorylated by Src family kinases (Huang *et al.*, 1998). This observation is consistent with a previous deletion analysis of cortactin (Hering & Sheng, 2003), suggesting the dispensable nature of the SH3 domain and the tyrosine phosphorylation sites for spine localization in mature neurons. However, dynamic redistribution of cortactin may still be regulated by SH3 domain and by phosphorylation, especially during development and synapse maturation. To evaluate this possibility, we next utilized time-lapse imaging of cortactin–ECFP to identify extracellular molecular cues effective for its redistribution in dendrites.

BDNF-dependent redistribution of cortactin toward the postsynaptic sites

To reveal signalling pathways important for maturation-dependent translocation of cortactin toward the postsynaptic sites, we analysed the redistribution of cortactin–ECFP after selective activation of signalling pathways using exogenous application of growth factors and neurotransmitters. For this purpose, we utilized relatively immature neurons at 12–16 days after plating. These neurons are in the process of developmental change in cortactin distribution and are expected to be more responsive to the exogenously applied extracellular ligands. We identified BDNF as the most potent growth factor for cortactin redistribution (Fig. 4A). Simultaneous time-lapse imaging of cortactin–ECFP and PSD-95–EYFP revealed cortactin accumulation at the pre-existing postsynaptic sites (Fig. 4B). Cortactin redistribution was not driven by actin reorganization *per se*, because EGFP–actin did not form clusters at the sites of cortactin accumulation (Fig. 4C). This effect of BDNF on cortactin redistribution was blocked by the tyrosine kinase antagonist K252a (Fig. 4E) and could not be induced by the same concentration of NGF and NT-3 (Fig. 4D). The effect of BDNF was less evident in mature hippocampal neurons maintained for > 20 days in culture (5.6 ± 3.9% increase in fluorescence intensity 60 min after BDNF application; $P > 0.05$, $n = 5$). Analysis of cortactin mutants showed that the C-terminal SH3 domain is important for BDNF-dependent cortactin redistribution (Fig. 4E). Binding of

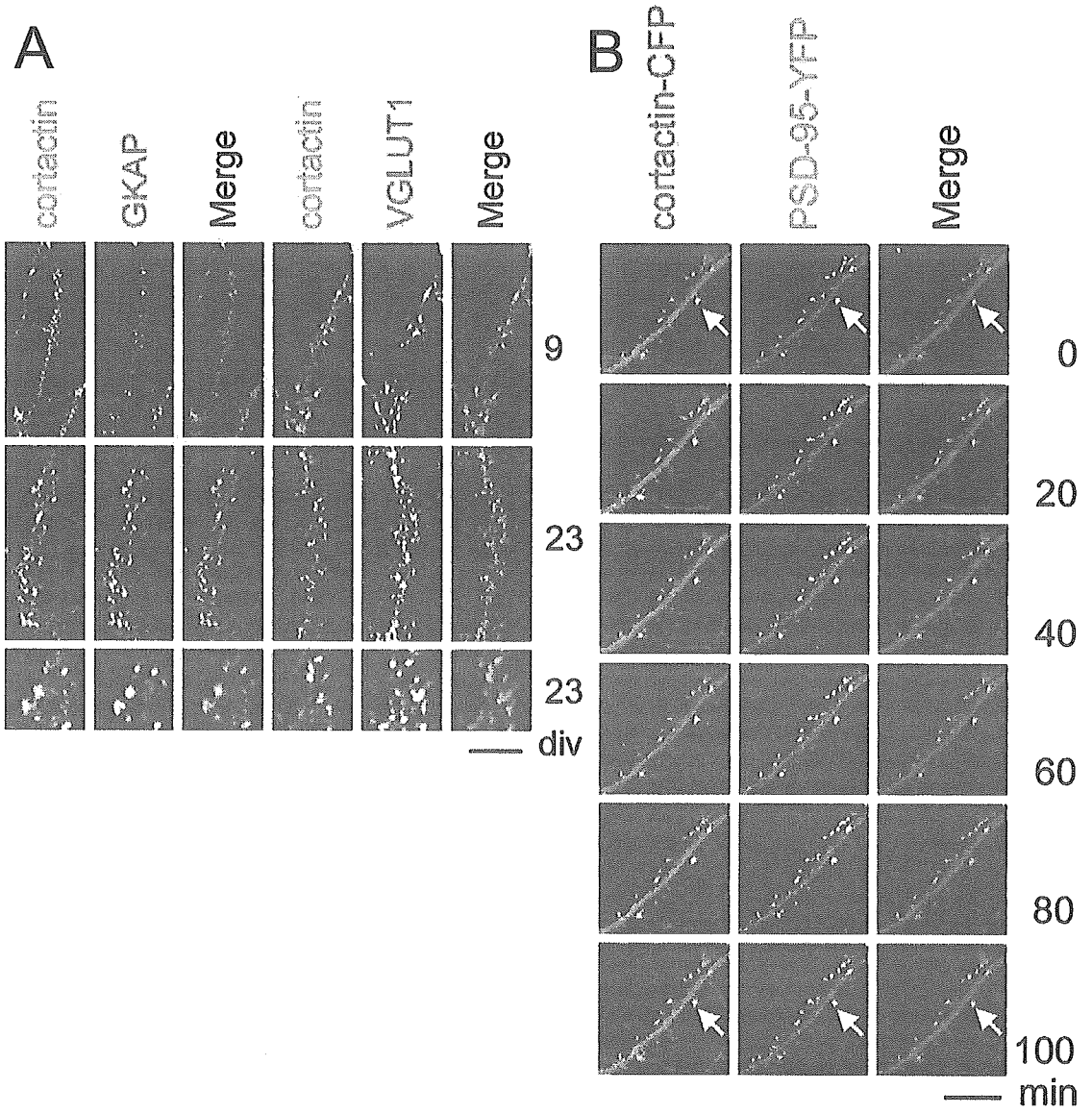

FIG. 1. Localization and dynamic behaviour of cortactin. (A) Developemental redistribution of cortactin from nonsynaptic cytoplasm to postsynaptic sites. Hippocampal neurons at 9 and 23 DIV were stained with anticortactin antibody together with a postsynaptic marker (GKAP) and a marker for the excitatory presynaptic component (VGLUT1). In neurons at 23 DIV, extensive overlap of cortactin clusters with GKAP clusters was observed. (B) Time-lapse imaging of cortactin–ECFP and PSD-95–EYFP in mature hippocampal neurons at 21 DIV. Cortactin–ECFP was localized at dendritic spines together with PSD-95–EYFP (arrows) without extensive remodeling within the observation period. Scale bars, 10 μm (B and lower magnification views in A), 5 μm (higher magnification views in A).

BDNF to trkB receptors can induce activation of both mitogen-activated protein (MAP) kinase and phosphoinositide-3 (PI3) kinase. BDNF-dependent redistribution of cortactin was selectively blocked by the MAP–Erk kinase inhibitor PD098059 but not by the PI3 kinase inhibitor LY294002 (Fig. 4E), suggesting a dominant role of MAP kinase activation in this process.

NMDA-dependent redistribution of cortactin away from the postsynaptic sites

It is possible that cortactin localization to the postsynaptic sites can be negatively regulated by exogenous ligands distinct from BDNF. A previous study reported that NMDA receptor activation induces loss of cortactin from spines (Hering & Sheng, 2003). To evaluate this phenomenon in our culture system, we stimulated cortactin–ECFP-expressing neurons at 18–22 days *in vitro* (DIV) with a low dose of NMDA. Prolonged activation of NMDA receptors induced gradual loss of cortactin–ECFP from spines (Fig. 5A). The Src family tyrosine kinase inhibitor PP2 prevented this redistribution (Fig. 5B) and the triple mutant of tyrosine phosphorylation sites did not show NMDA-dependent redistribution (Fig. 5C). A decrease in the cortactin–ECFP signal from spines was also observed in immature neurons (12–16 DIV) but the effect was less extensive (12.8 ± 3.4% decrease in fluorescence intensity 60 min after NMDA application; $P < 0.05$, $n = 5$). To activate Src family tyrosine kinases directly, we treated

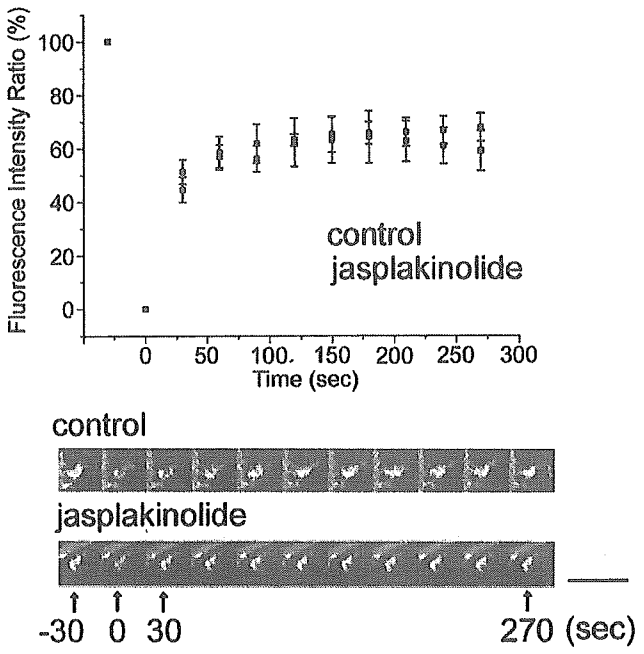

FIG. 2. FRAP analysis of cortactin tagged with ECFP. Mature hippocampal neurons at 20 DIV expressing cortactin–ECFP were analysed for steady-state turnover rate of cortactin using FRAP. Rapid recovery of fluorescence was observed in both control preparations and those treated with jasplakinolide to stabilize F-actin (n = 10 for both control and jasplakinolide-treated preparations). Scale bar, 3 μm.

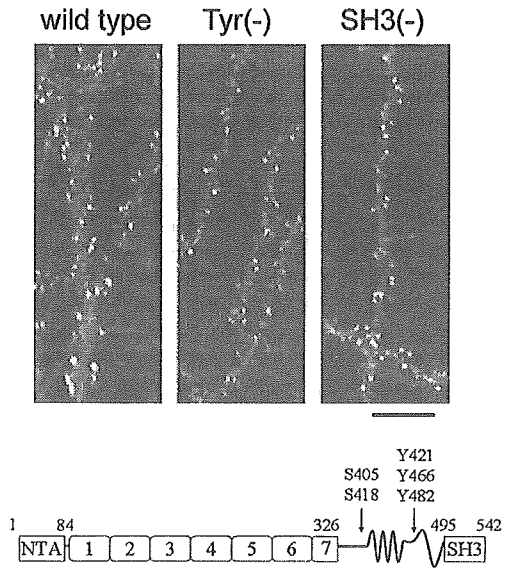

FIG. 3. Synaptic localization of mutant cortactin molecules tagged with ECFP. Wild-type cortactin molecules or cortactin mutants tagged with ECFP were expressed in mature hippocampal neurons at 22 DIV. Mutant cortactin molecules with either three alanine substitutions of tyrosine residues or deletion of the SH3 domain were localized in the dendritic spines. Scale bar, 10 μm.

neuronal culture with 100 μM of H_2O_2 (Martinez *et al.*, 2003). This treatment induced both dissociation of endogenous cortactin from postsynaptic sites immunopositive for anti-Homer antibody (Fig. 5D) and a dramatic increase in tyrosine phosphorylation of cortactin (Fig. 5F). Dissociation of immunopositive clusters was specific to cortactin, and clustering of Homer proteins was not affected (Fig. 5E). The H_2O_2-induced redistribution was dependent on activation of Src family kinases, because the Src family kinase blocker PP2 inhibited the effect of H_2O_2 (Fig. 5D and E).

Roles of endogenous BDNF and glutamate receptor activation on cortactin redistribution

Our results indicate that exogenous application of BDNF and NMDA induced redistribution of cortactin in opposite directions. To see whether endogenously released BDNF plays a role in cortactin redistribution to the postsynaptic sites during development, we maintained hippocampal neuronal culture in the presence of trkB–immunogloblin G (IgG) for 5 days (from 12 to 16 days after plating) and examined colocalization of cortactin-immunopositive clusters with PSD-95 clusters. After trkB–IgG treatment, the percentage of overlapping clusters was reduced to 67% of control (Fig. 6A and B). If baseline activation of NMDA receptors in cultured neurons plays a role in trkB–IgG-induced reduction of postsynaptic cortactin clusters, inhibition of NMDA receptor activation could be expected to antagonize the net effect of trkB–IgG. Indeed, we observed a reversal of the trkB–IgG-induced reduction of cortactin clusters by treatment with the NMDA receptor antagonist APV (Fig. 6B). These results collectively indicate that activation of trkB receptors by endogenous BDNF is important in the re-organization of postsynaptic cortactin-associated PSD complex. Furthermore, this BDNF-dependent maturation process is negatively modulated by basal NMDA receptor activity, thereby identifying cortactin as a critical signalling sensor involved in regulation of PSD remodeling during development. To determine whether blockade of BDNF signalling can acutely eliminate preassembled cortactin clusters in the postsynaptic sites, we monitored the behaviour of cortactin–ECFP after application of trkB–IgG. We could not detect cortactin–ECFP redistribution within 3 h after trkB–IgG treatment (data not shown), indicating resistance of cortactin clusters to the depletion of endogenous BDNF over a time scale of several hours.

Discussion

In this study we have shown BDNF-dependent redistribution of cortactin. Cortactin redistribution is mediated by trkB receptor activation because this redistribution could not be induced by NGF or NT-3 application and was blocked by the tyrosine kinase inhibitor K252a. In fibroblasts, stimulation of receptor tyrosine kinases such as platelet-derived growth factor receptors and insulin receptors leads to translocation of cortactin to the site of membrane ruffling, and activation of the small GTPase Rac is involved in this process (Du Weed *et al.*, 1998). Inhibition of PI3 kinase activity suppresses the induction of membrane ruffling by growth factors in fibroblasts (Nobes *et al.*, 1995) and it is likely that cortactin redistribution in fibroblasts is also regulated via the PI3 kinase-dependent pathway. Pharmacological analysis revealed that BDNF-dependent cortactin redistribution required subsequent activation of the MAP kinase pathway but is not dependent on activation of PI3 kinase, suggesting neuron-specific mechanisms of cortactin translocation. Biochemical analysis revealed Erk-dependent phosphorylation of cortactin at residues S405 and S418, which are located within the proline-rich region of cortactin (Campbell *et al.*, 1999). It is postulated that the SH3 domain of cortactin is engaged in intramolecular association with

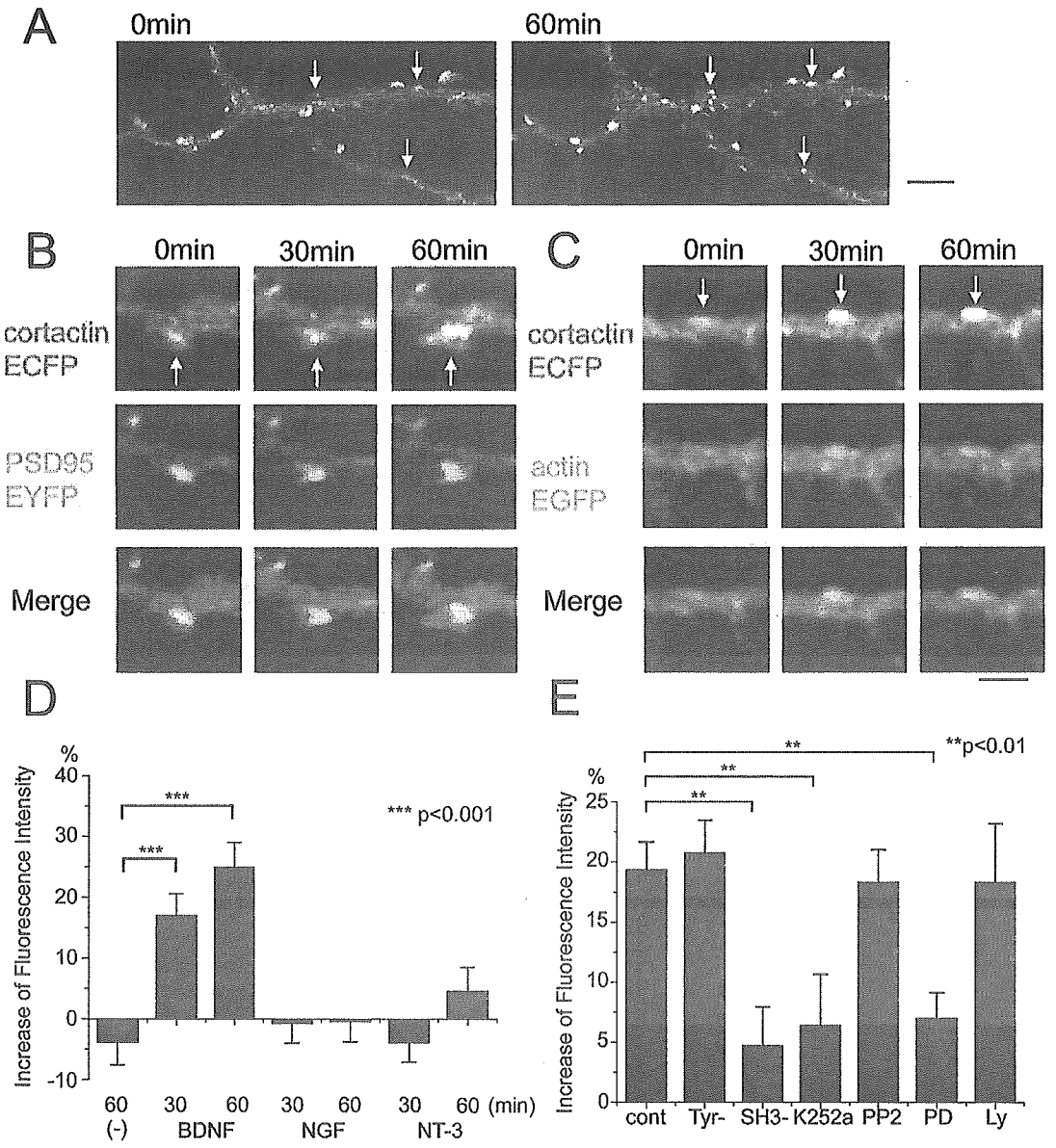

FIG. 4. Redistribution of cortactin–ECFP by application of BDNF. (A) Time-lapse imaging of cortactin–ECFP-expressing hippocampal neurons after BDNF application. Formation of new clusters of cortactin–ECFP was observed (arrows). (B) Accumulation of cortactin in the pre-existing clusters of PSD-95–EYFP. Simultaneous time-lapse observation of cortactin–ECFP and PSD-95–EYFP revealed redistribution of cortactin to the postsynaptic sites identified by PSD-95–EYFP fluorescence (arrows). (C) Simultaneous observation of cortactin–ECFP and EGFP–actin revealed independent behaviour of cortactin and actin (arrows). (D) Effects of neurotrophins on clustering of cortactin–ECFP. Cortactin redistribution was selectively induced by BDNF ($n = 9$ for control, $n = 16$ for BDNF, $n = 10$ for NGF and NT-3). (E) Effects of protein kinase inhibitors and mutation constructs on cortactin redistribution 60 min after BDNF application ($n = 34$ for control, $n = 10$ for triple phenylalanine mutant (Tyr-), $n = 9$ for deletion mutant of SH3 domain (SH3-), $n = 10$ for K252a treatment, $n = 10$ for PP2 treatment, $n = 10$ for PD098059 treatment (PD) and $n = 10$ for LY294002 treatment (Ly). Scale bars, 5 μm (A), 2 μm (B and C).

the proline-rich region (Martinez-Quiles *et al.*, 2004). Erk-dependent phosphorylation of S405 and S418 within the proline-rich region of cortactin may disrupt intramolecular interactions and enhance availability of the SH3 domain to form intermolecular association. This model is consistent with our observation that the cortactin mutant lacking the SH3 domain does not show BDNF-dependent redistribution to the postsynaptic sites. Shank, dynamin and N-WASP are possible binding partners for the cortactin SH3 domain at the postsynaptic cytoplasm (Naisbitt *et al.*, 1999; McNiven *et al.*, 2000; Martinez-Quiles *et al.*, 2004). Among these, interaction with Shank should be important in the regulation of cortactin dynamics. We identified a large stable fraction of cortactin–ECFP by FRAP analysis and the localization of this fraction within spines cannot be explained by interaction with the actin cytoskeleton which, itself, turns over in a time scale of minutes (Star *et al.*, 2002). Shank is a component of the stable PSD scaffolds and interaction with Shank may reduce turnover rate of cortactin at the postsynaptic sites. We also observed accumulation of cortactin within spines by overexpression of Shank2–EGFP (J. Iki and S. Okabe, unpublished observation). It has been reported that morphological maturation of dendritic spines

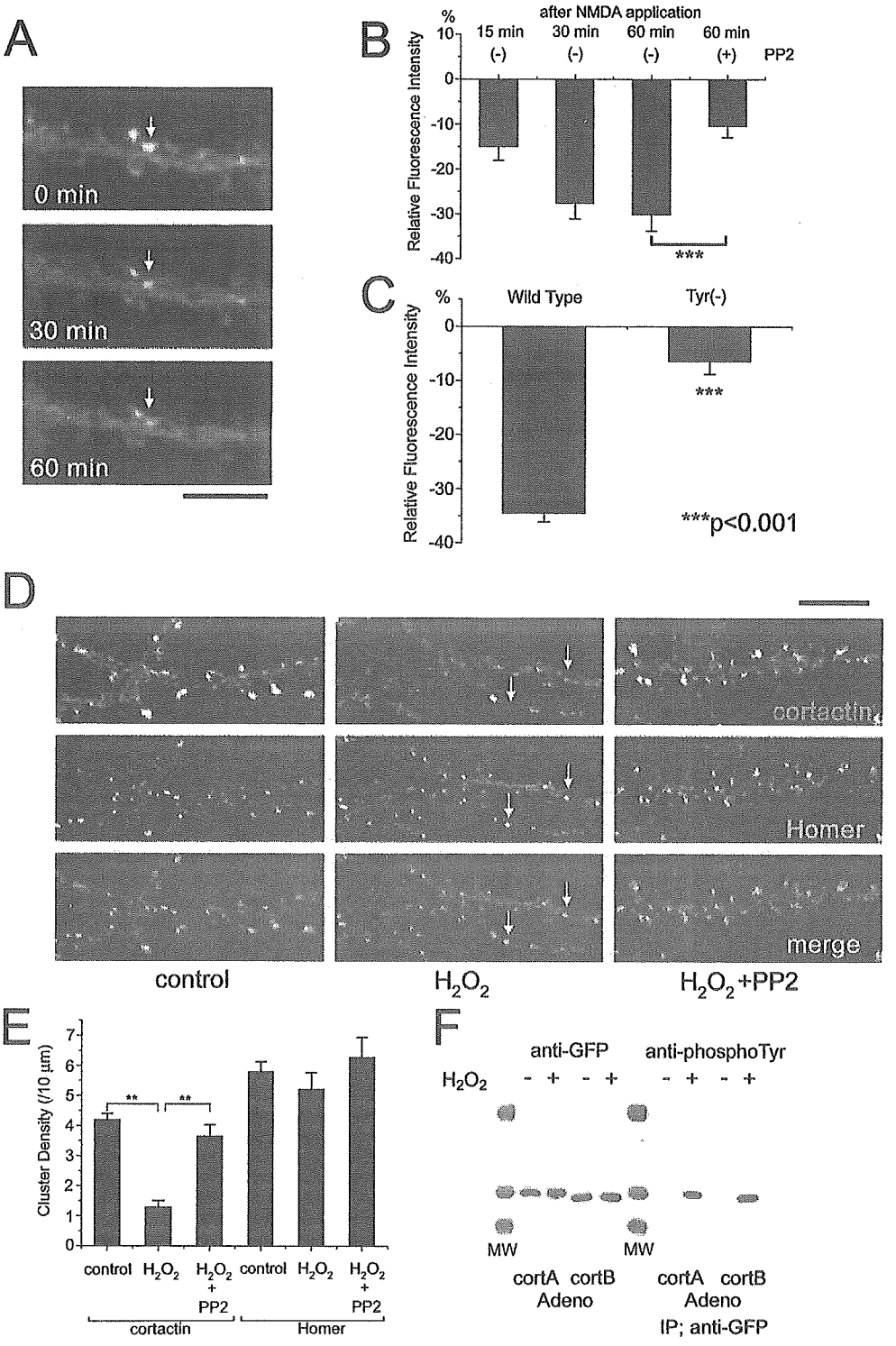

FIG. 5. Redistribution of cortactin by application of NMDA and H_2O_2. (A) Redistribution of cortactin–ECFP after NMDA application. Gradual loss of cortactin–ECFP from dendritic spines was observed (arrows). (B) Effects of NMDA receptor activation on cortactin localization at the postsynaptic sites. Decrease of cortactin at the postsynaptic sites was prevented by PP2 treatment ($n = 10$). (C) Mutations of three tyrosine residues (Y421F, Y466F and Y482F) abolished redistribution of cortactin 60 min after NMDA application ($n = 10$). (D) Immunocytochemistry of neurons treated with H_2O_2 for 60 min using anticortactin and anti-Homer antibody. H_2O_2 treatment induced selective loss of cortactin from the postsynaptic sites and increased the number of Homer clusters without cortactin immunoreactivity (arrows). (E) Quantitative analysis of cluster density in neurons treated with H_2O_2 for 60 min. Selective reduction in the density of cortactin clusters was observed ($n = 20$ for each treatment). (F) Tyrosine phosphorylation of cortactin–ECFP by H_2O_2 treatment. Primary hippocampal neurons infected with recombinant adenoviruses expressing cortactin A–ECFP and cortactin B–ECFP were treated with H_2O_2 for 60 min, extracted and immunoprecipitated with anti-GFP antibody. Molecular weight markers (MW) correspond to 211, 122 and 80 kDa. Scale bars, 5 μm (A), 10 μm (D).

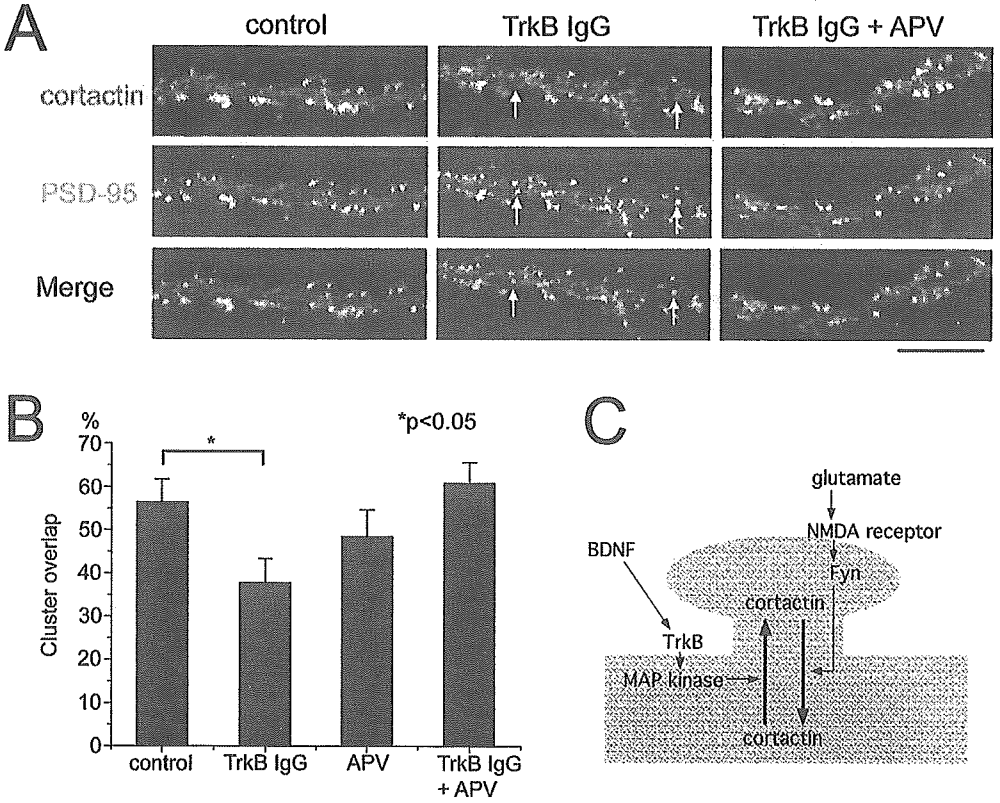

FIG. 6. Interaction of BDNF-dependent and NMDA-dependent signalling in cortactin redistribution. (A) Inhibition of endogenous BDNF activity by trkB–IgG. Application of trkB–IgG for 5 days (12–16 DIV) reduced cortactin clusters colocalized with PSD-95 (arrows). This effect of trkB–IgG was rescued by inhibiting NMDA receptor activity with APV. (B) Quantification of PSD-95 clusters with cortactin immunoreactivity. Treatment of hippocampal neurons with trkB–IgG reduced the clustering of cortactin at the PSD-95-positive postsynaptic sites (n = 30 for each culture condition). (C) A model of BDNF- and NMDA-dependent signalling on cortactin redistribution. Binding of BDNF to trkB receptors activates tyrosine kinase activity and subsequently induces MAP kinase activation. MAP kinase directly phosphorylates cortactin within the proline-rich region, dissociates intramolecular association and facilitates SH3 domain-dependent association at the postsynaptic site. Synaptic transmission together with membrane depolarization activates NMDA receptors and positively regulates Src family kinases including Fyn at the postsynaptic site. Tyrosine phosphorylation of cortactin reduces its activity to initiate actin polymerization and possibly results in dissociation from the postsynaptic actin cytoskeleton. Alternatively, tyrosine phosphorylation may reduce the affinity of the cortactin SH3 domain for Shank. Scale bar, 10 μm.

can be induced by overexpression of Shank in hippocampal neurons (Sala *et al.*, 2001). Recruitment of cortactin to dendritic spines through interaction with Shank may be important in BDNF-dependent regulation of postsynaptic maturation.

It has been reported that NMDA receptor stimulation induces redistribution of cortactin from spines to dendritic shafts (Hering & Sheng, 2003). In our culture system we could reproduce this observation by using a protocol of prolonged exposure of hippocampal neurons to a low dose of NMDA in the presence of the AMPA receptor antagonist CNQX and the sodium channel blocker TTX. Although the previous report indicated correlated redistribution of F-actin after NMDA treatment, we did not observe profound remodeling of actin filaments with our protocol of NMDA treatment (data not shown). Furthermore, we observed suppression of NMDA-dependent cortactin redistribution by the Src family kinase inhibitor PP2, and the triple phenylalanine mutant of tyrosine residues was resistant to the NMDA stimulation protocol. These results indicate the possibility of tyrosine phosphorylation of cortactin by NMDA stimulation and subsequent release of cortactin from the postsynaptic sites. Indeed, direct activation of Src family kinases by H_2O_2 results in a similar redistribution of cortactin from the postsynaptic sites. There are two possible mechanisms for tyrosine phosphorylation-dependent cortactin redistribution. One possibility is that phosphorylation of cortactin by Src family kinases negatively regulates initiation of actin polymerization. A recent biochemical study showed inhibition of cortactin-dependent N-WASP activation by Src phosphorylation of cortactin (Martinez-Quiles *et al.*, 2004). It has been reported that CagA protein of *Helicobacter pylori* induces both cortactin dephosphorylation and recruitment of cortactin to actin-rich cellular protrusions (Selbach *et al.*, 2003). This observation is consistent with the idea that dephosphorylation of tyrosine residues in cortactin is paralleled with cortactin activity to initiate actin polymerization via interaction with WASP family proteins and its redistribution to the actin-rich motile domains. Another possible mechanism of cortactin redistribution from the postsynaptic sites is reduced affinity of cortactin to Shank by tyrosine phosphorylation. Interaction of the cortactin SH3 domain to N-WASP is regulated by tyrosine phosphorylation (Martinez-Quiles *et al.*, 2004) and it is possible that SH3 domain–mediated association of cortactin to Shank is also negatively regulated by Src phosphorylation. These two possibilities should be clarified in the future by manipulating actin polymerization during activation of NMDA receptors in primary neurons.

Expression and release of BDNF is known to be enhanced by neuronal activity and has been shown to be important in maturation of GABAergic interneurons (Rutherford *et al.*, 1997; Kohara *et al.*,

2003). There is also accumulating evidence suggesting roles of BDNF in the development of dendritic arborizations and spines of pyramidal neurons (McAllister *et al.*, 1995; Horch & Katz, 2002). Knockdown of cortactin has been shown to induce depletion of dendritic spines, suggesting critical involvement of cortactin in postsynaptic morphogenesis (Hering & Sheng, 2003). We observed reduced postsynaptic content of cortactin by blocking endogenous BDNF activity. Thus cortactin-dependent actin reorganization possibly underlies BDNF-dependent regulation of postsynaptic structure. We noticed a relatively slow time-course of cortactin redistribution away from the postsynaptic sites by blocking endogenous BDNF. There are several possible explanations for this observation. First, the time-course of cortactin dissociation from the postsynaptic sites might be slower than its assembly. It is also possible that the effect of trkB–IgG is through the enhancement of NMDA-dependent elimination of newly formed cortactin clusters. In this case, preexisting cortactin clusters can persist after application of trkB–IgG and the effect of BDNF depletion is mainly due to destabilization of new clusters during the course of development. Finally, it should be also possible that trkB–IgG treatment can induce suppression of inhibitory neuronal function, resulting in enhancement of excitatory circuits. This up-regulation of glutamatergic neurons might play a role in cortactin redistribution. However, our preliminary data indicate unaltered morphology of glutamic acid decarboxylase-positive neurons 5 days after trkB–IgG treatment, suggesting direct effects of BDNF depletion on the postsynaptic cortactin.

We have provided evidence of negative regulation of BDNF-dependent cortactin redistribution by NMDA receptor activation. This result indicates the importance of the balance between BDNF signalling and NMDA receptor activation in cortactin distribution (Fig. 6C). During the period of synapse development, where synaptic activity is less prominent, it is likely that gradual cortactin accumulation at the postsynaptic site is favoured in a BDNF-dependent manner. However, such a mechanism is counterbalanced, once mature synaptic terminals are formed and robust NMDA receptor activation can be achieved, by Src kinase activity which presumably then negatively regulates synaptic cortactin redistribution. Assuming enhancement of synaptic transmission by cortactin, dual regulation of cortactin redistribution by BDNF and NMDA receptor activation will provide a negative feedback mechanism which may function to stabilize excitatory synaptic transmission during development.

Acknowledgements

We thank Dr K. Sobue and M. Watanabe for antibodies, Dr H. Okado for preparation of recombinant adenoviruses and I. Kawabata for preparation of primary hippocampal neurons. This work was supported by grants from the Ministry of Education, Science, Sports, Culture and Technology of Japan, the Core Research for Evolutional Science and Technology of Japan Science and Technology Agency and the Human Frontier Science Program.

Abbreviations

AMPA, α-amino-3-hydroxy-5-methyl-isoxazolepropionic acid; APV, 2-amino-5-phosphonovaleric acid; BDNF, brain-derived neurotrophic factor; CNQX, 6-cyano-7-nitroquinoxaline-2,3-dione; DIV, days *in vitro*; ECFP, enhanced cyan fluorescent protein; EGFP, enhanced green fluorescent protein; EYFP, enhanced yellow fluorescent protein; FRAP, fluorescence recovery after photobleaching; IgG, immunogloblin G; MAP, mitogen-activated protein; NMDA, *N*-methyl-D-aspartate; NT-3, neurotrophin-3; PI3, phosphatidylinositol 3; PP2, 4-amino-5-(4-chlorophenyl)-7-(t-butyl)pyrazolo[3,4-d]pyrimidine; PSD, postsynaptic density; TTX, tetrodotoxin; WASP, Wiskott–Aldrich syndrome protein.

References

Allison, D.W., Gelfand, V.I., Spector, I. & Craig, A.M. (1998) Role of actin in anchoring postsynaptic receptors in cultured hippocampal neurons: differential attachment of NMDA versus AMPA receptors. *J. Neurosci.*, **18**, 2423–2436.

Bibel, M. & Barde, Y.A. (2000) Neurotrophins: key regulators of cell fate and cell shape in the vertebrate nervous system. *Genes Dev.*, **14**, 2919–2937.

Boeckers, T.M., Kreutz, M.R., Winter, C., Zuschratter, W., Smalla, K.H., Sanmarti-Vila, L., Wex, H., Langnaese, K., Bockmann, J., Garner, C.C. & Gundelfinger, E.D. (1999) Proline-rich synapse-associated protein-1/cortactin binding protein 1 (ProSAP1/CortBP1) is a PDZ-domain protein highly enriched in the postsynaptic density. *J. Neurosci.*, **19**, 6506–6518.

Campbell, D.H., Sutherland, R.L. & Daly, R.J. (1999) Signaling pathways and structural domains required for phosphorylation of EMS1/cortactin. *Cancer Res.*, **59**, 5376–5385.

Du Weed, S.A.Y. & Parsons, J.T. (1998) Translocation of cortactin to the cell periphery is mediated by the small GTPase Rac1. *J. Cell Sci.*, **111**, 2433–2443.

Ebihara, T., Kawabata, I., Usui, S., Sobue, K. & Okabe, S. (2003) Synchronized formation and remodeling of postsynaptic densities: long-term visualization of hippocampal neurons expressing postsynaptic density proteins tagged with green fluorescent protein. *J. Neurosci.*, **23**, 2170–2181.

Furuyashiki, T., Arakawa, Y., Takemoto-Kimura, S., Bito, H. & Narumiya, S. (2002) Multiple spatiotemporal modes of actin reorganization by NMDA receptors and voltage-gated Ca^{2+} channels. *Proc. Natl Acad. Sci. USA*, **99**, 14458–14463.

Halpain, S., Hipolito, A. & Saffer, L. (1998) Regulation of F-actin stability in dendritic spines by glutamate receptors and calcineurin. *J. Neurosci.*, **18**, 9835–9844.

Hering, H. & Sheng, M. (2003) Activity-dependent redistribution and essential role of cortactin in dendritic spine morphogenesis. *J. Neurosci.*, **23**, 11759–11769.

Horch, H.W. & Katz, L.C. (2002) BDNF release from single cells elicits local dendritic growth in nearby neurons. *Nat. Neurosci.*, **5**, 1177–1184.

Huang, C., Liu, J., Haudenschild, C.C. & Zhan, X. (1998) The role of tyrosine phosphorylation of cortactin in the locomotion of endothelial cells. *J. Biol. Chem.*, **273**, 25770–25776.

Itami, C., Kimura, F., Kohno, T., Matsuoka, M., Ichikawa, M., Tsumoto, T. & Nakamura, S. (2003) BDNF-dependent unmasking of "silent" synapses in the developing mouse barrel cortex. *Proc. Natl. Acad. Sci. USA*, **100**, 13069–13074.

Iwasato, T., Datwani, A., Wolf, A.M., Nishiyama, H., Taguchi, Y., Tonegawa, S., Knopfel, T., Erzurumlu, R.S. & Itohara, S. (2000) Cortex-restricted disruption of NMDAR1 impairs neuronal patterns in the barrel cortex. *Nature*, **406**, 726–731.

Kohara, K., Kitamura, A., Adachi, N., Nishida, M., Itami, C., Nakamura, S. & Tsumoto, T. (2003) Inhibitory but not excitatory cortical neurons require presynaptic brain-derived neurotrophic factor for dendritic development, as revealed by chimera cell culture. *J. Neurosci.*, **23**, 6123–6131.

Kohara, K., Kitamura, A., Morishima, M. & Tsumoto, T. (2001) Activity-dependent transfer of brain-derived neurotrophic factor to postsynaptic neurons. *Science*, **291**, 2419–2423.

Li, Y., Erzurumlu, R.S., Chen, C., Jhaveri, S. & Tonegawa, S. (1994) Whisker-related neuronal patterns fail to develop in the trigeminal brainstem nuclei of NMDAR1 knockout mice. *Cell*, **76**, 427–437.

Manabe, T. (2002) Does BDNF have pre- or postsynaptic targets? *Science*, **295**, 1651–1653.

Martinez, M.C., Ochiishi, T., Majewski, M. & Kosik, K.S. (2003) Dual regulation of neuronal morphogenesis by a delta-catenin-cortactin complex and Rho. *J. Cell Biol.*, **162**, 99–111.

Martinez-Quiles, N., Ho, H.Y., Kirschner, M.W., Ramesh, N. & Geha, R.S. (2004) Erk/Src phosphorylation of cortactin acts as a switch on-switch off mechanism that controls its ability to activate N-WASP. *Mol. Cell Biol.*, **24**, 5269–5280.

McAllister, A.K., Lo, D.C. & Katz, L.C. (1995) Neurotrophins regulate dendritic growth in developing visual cortex. *Neuron*, **15**, 791–803.

McNiven, M.A., Kim, L., Krueger, E.W., Orth, J.D., Cao, H. & Wong, T.W. (2000) Regulated interactions between dynamin and the actin-binding protein cortactin modulate cell shape. *J. Cell Biol.*, **151**, 187–198.

Naisbitt, S., Kim, E., Tu, J.C., Xiao, B., Sala, C., Valtschanoff, J., Weinberg, R.J., Worley, P.F. & Sheng, M. (1999) Shank, a novel family of postsynaptic density proteins that binds to the NMDA receptor/PSD-95/GKAP complex and cortactin. *Neuron*, **23**, 569–582.

Nakanishi, S. (1992) Molecular diversity of glutamate receptors and implications for brain function. *Science*, **258**, 597–603.

Nobes, C.D., Hawkins, P., Stephens, L. & Hall, A. (1995) Activation of the small GTP-binding proteins rho and rac by growth factor receptors. *J. Cell Sci.*, **108**, 225–233.

Okabe, S., Kim, H.D., Miwa, A., Kuriu, T. & Okado, H. (1999) Continual remodeling of postsynaptic density and its regulation by synaptic activity. *Nat. Neurosci.*, **2**, 804–811.

Okabe, S., Miwa, A. & Okado, H. (2001) Spine formation and correlated assembly of presynaptic and postsynaptic molecules. *J. Neurosci.*, **21**, 6105–6114.

Okamoto, K., Nagai, T., Miyawaki, A. & Hayashi, Y. (2004) Rapid and persistent modulation of actin dynamics regulates postsynaptic reorganization underlying bidirectional plasticity. *Nat. Neurosci.*, **7**, 1104–1112.

Racz, B. & Weinberg, R.J. (2004) The subcellular organization of cortactin in hippocampus. *J. Neurosci.*, **24**, 10310–10317.

Rutherford, L.C., DeWan, A., Lauer, H.M. & Turrigiano, G.G. (1997) Brain-derived neurotrophic factor mediates the activity-dependent regulation of inhibition in neocortical cultures. *J. Neurosci.*, **17**, 4527–4535.

Sala, C., Piech, V., Wilson, N.R., Passafaro, M., Liu, G. & Sheng, M. (2001) Regulation of dendritic spine morphology and synaptic function by Shank and Homer. *Neuron*, **31**, 115–130.

Selbach, M., Moese, S., Hurwitz, R., Hauck, C.R., Meyer, T.F. & Backert, S. (2003) The Helicobacter pylori CagA protein induces cortactin dephosphorylation and actin rearrangement by c-Src inactivation. *EMBO J.*, **22**, 515–528.

Shen, K. & Meyer, T. (1999) Dynamic control of CaMKII translocation and localization in hippocampal neurons by NMDA receptor stimulation. *Science*, **284**, 162–166.

Star, E.N., Kwiatkowski, D.J. & Murthy, V.N. (2002) Rapid turnover of actin in dendritic spines and its regulation by activity. *Nat. Neurosci.*, **5**, 239–246.

Thoenen, H. (1995) Neurotrophins and neuronal plasticity. *Science*, **270**, 593–598.

Usui, S., Konno, D., Hori, K., Maruoka, H., Okabe, S., Fujikado, T., Tano, Y. & Sobue, K. (2003) Synaptic targeting of PSD-Zip45 (Homer 1c) and its involvement in the synaptic accumulation of F-actin. *J. Biol. Chem.*, **278**, 10619–10628.

Watanabe, M., Fukaya, M., Sakimura, K., Manabe, T., Mishina, M. & Inoue, Y. (1998) Selective scarcity of NMDA receptor channel subunits in the stratum lucidum (mossy fibre-recipient layer) of the mouse hippocampal CA3 subfield. *Eur. J. Neurosci.*, **10**, 478–487.

Wu, H. & Parsons, J.T. (1993) Cortactin, an 80/85-kilodalton pp60src substrate, is a filamentous actin-binding protein enriched in the cell cortex. *J. Cell Biol.*, **120**, 1417–1426.

Wu, H., Reynolds, A.B., Kanner, S.B., Vines, R.R. & Parsons, J.T. (1991) Identification and characterization of a novel cytoskeleton-associated pp60src substrate. *Mol. Cell Biol.*, **11**, 5113–5124.

Wyszynski, M., Lin, J., Rao, A., Nigh, E., Beggs, A.H., Craig, A.M. & Sheng, M. (1997) Competitive binding of alpha-actinin and calmodulin to the NMDA receptor. *Nature*, **385**, 439–442.

Zafra, F., Hengerer, B., Leibrock, J., Thoenen, H. & Lindholm, D. (1990) Activity dependent regulation of BDNF and NGF mRNAs in the rat hippocampus is mediated by non-NMDA glutamate receptors. *EMBO J.*, **9**, 3545–3550.

Available online at www.sciencedirect.com
SCIENCE DIRECT®
Neuroscience Research 51 (2005) 417–425
Neuroscience Research
www.elsevier.com/locate/neures

Two-dimensional neural activity mapping of the entire population of hippocampal CA1 pyramidal cells responding to fear conditioning

Koutarou Inoue[a,b,1], Yugo Fukazawa[a,2], Akihiko Ogura[b], Kaoru Inokuchi[a,*]

[a] *Mitsubishi Kagaku Institute of Life Sciences (MITILS), 11 Minamiooya, Machida, Tokyo 194-8511, Japan*
[b] *Department of Biology, Osaka University of Graduate School of Science, Toyonaka, Osaka 560-0043, Japan*

Received 16 November 2004; accepted 14 December 2004
Available online 15 January 2005

Abstract

The hippocampus is involved in the encoding, storage, and retrieval of memory. Here, we have developed a novel mapping method for detecting the distribution of neural activity of the entire population of pyramidal cells in the hippocampal CA1 and subiculum regions, where expression profiles of *Arc* mRNA were used as an indicator of neural activity. The spherical pyramidal cell layer of the intact hippocampus was flattened into a two-dimensional plane, which was then serially sectioned in parallel with the plane to make tangential sections. Tangential sections were hybridized with an *Arc* cRNA probe and *Arc* signals from serial tangential sections were stacked and displayed on a two-dimensional plane, allowing one to easily visualize the neural activity of all pyramidal cells. We applied this method to the hippocampus of rats that had experienced contextual fear conditioning, which requires hippocampal function. We observed a net shift of *Arc* signals from dorsal to ventral CA1/subiculum with an interval prolongation to reconditioning after the initial conditioning. The reconditioning-revealed shift may reflect a reorganization process, which takes place during the period between initial conditioning and reconditioning, in the CA1/subiculum neural network that represents the neural storage and/or retrieval of the contextual fear conditioning.

Keywords: Contextual fear conditioning; Two-dimensional map; Ventral hippocampus; *Arc* gene expression; Tangential section; Neural circuit; Memory consolidation; Memory retrieval

1. Introduction

Information processing in the brain is mediated by neural networks that, upon experience, change their circuits in a plastic manner. Memory is thought to be represented on these neural networks. It is therefore very important to identify such networks and describe changes in networks during memory acquisition, consolidation, and retrieval. Generally, electrophysiological recording, histological analysis, and functional imaging are used to analyze neural networks involved in information processing during memory formation. Although these methods have a number of merits, it is quite difficult by these methods to display the entire neural activity of a given brain region such as the hippocampus, in spatially high resolution, for example, at the single cell level.

The hippocampus is involved in encoding, storage and retrieval of associations responsible for episodic memory, as well as spatial memory (O'Keefe and Dostrovsky, 1971; Morris et al., 1982; Brown and Aggleton, 2001; Eichenbaum, 2004). The hippocampus consists of four major subfields, the subiculum, CA1, CA3, and dentate gyrus. These subfields seem to be involved in distinct aspects of informational processing (Lisman, 1999). Both anatomical and lesion studies indicate that the dorsal and ventral parts of the hippocampus are functionally distinct (Maren et al., 1997; Moser and Moser, 1998; Hampson et al., 1999; Richmond et al., 1999; Kjelstrup et al., 2002; Bannerman et al., 2003). The dorsal hippocampus receives its input

* Corresponding author. Tel.: +81 427 246 318; fax: +81 427 246 318.
E-mail address: kaoru@libra.ls.m-kagaku.co.jp (K. Inokuchi).
[1] Present address: Age Dimension Research Center, National Institute of Advanced Industrial Science and Technology (AIST), Tsukuba, Ibaraki 305-8566, Japan.
[2] Present address: Division of Cerebral Structure, National Institute for Physiological Sciences, Okazaki 444-8585, Japan.

0168-0102/$ – see front matter © 2004 Elsevier Ireland Ltd and the Japan Neuroscience Society. All rights reserved.
doi:10.1016/j.neures.2004.12.012

primarily from the lateral portions of the entorhinal cortex, which receives its major inputs from various sensory and associational neocortical areas. Thus, the dorsal hippocampus is proposed to be important, specifically for the processing of exteroceptive sensory information. On the other hand, the medial portions of the entorhinal cortex, which receive an input predominantly from structures such as the amygdala, project primarily to the ventral hippocampus, suggesting that the ventral hippocampus is more important for the processing of interoceptive sensory information and emotion (Amaral and Witter, 1995). Indeed, the dorsal hippocampus plays a central role in spatial memory, whereas the ventral hippocampus is required for contextual fear conditioning (Maren et al., 1997; Moser and Moser, 1998; Richmond et al., 1999; Pittenger et al., 2002).

Here, we developed a novel method to display neural activity of the entire population of CA1/subiculum pyramidal cells by two-dimensional mapping using stacked images of tangential sections, in which the mRNA expression of one of the immediate–early genes (IEGs), *Arc*, was used as an indicator of neural activity. Among IEGs that are induced during behavioral tasks, *Arc* gene induction in the hippocampal CA1 region is specifically linked to information processing rather than general neural activities such as motor activity, environmental novelty or responses to stress (Guzowski et al., 1999, 2001; Kelly and Deadwyler, 2003). Furthermore, *Arc* mRNA expression is most sensitive to changes in behavioral tasks compared to that of the other IEGs, c-*fos* and *zif268* (Guzowski et al., 2000). Antisense oligonucleotide-mediated suppression of the Arc protein impairs long-term memory consolidation without affecting task acquisition or short-term memory (Guzowski et al., 2000). These observations make *Arc* expression suitable for the representation of a neural circuit associated with information processing. We applied this method to rats that performed contextual fear conditioning, and found a net shift of neural activity from dorsal to ventral CA1/subiculum over time after the initial conditioning. This shift may reflect a change in neural circuit associated with information coding, storage, and/or retrieval.

2. Materials and methods

2.1. Subjects and behavioral procedures

All the animal experiments were carried out in accordance with the National Institutes of Health guide for the care and use of laboratory animals and were approved by the Animal Care and Use Committee of the Mitsubishi Kagaku Institute of Life Science (MITILS). Naive male Wistar ST rats (8–9 weeks, 280–300 g) were housed individually in cages with free access to food and water. They were maintained in a 12 h light:12 h dark cycle, with lights on at 9:00 a.m., under constant temperature (24 ± 1 °C) in a room with a clean air conditioning system. They were handled over 1 week and then experiments were carried out in a neighboring room with the same environmental conditions.

Contextual fear conditioning was performed in a conditioning chamber that was an observation box (32 cm × 22 cm × 22 cm) made of clear and gray polyvinylchloride plates. The floor of the chamber consisted of 28 stainless steel rods (0.4 cm diameter, spaced 1 cm apart) through which foot-shocks were delivered by a scrambled-foot-shock generator SGS 002 (Muromachi Kikai Co., Tokyo, Japan). The chamber was placed in a lighted room. The chamber was cleaned with ethanol (99.5%) and dried with a hair drier for a change of air before and after the occupancy of each rat. A video camera placed in front of the chamber recorded the behavior of each rat. A controller for conditioning was operated by a remote switch placed far from the conditioning chamber.

For both conditioning and reconditioning, each rat was placed in the chamber for 5 min, and freezing behavior was observed. Then, these rats received three electric foot-shocks (0.5 mA intensity, 1.0 s duration, 30 s interval), remained in the chamber for 2 min, and then were returned to their home cage (Fig. 1A). Freezing score was counted when a rat did not move at all for the first 3 s of every 5 s interval.

2.2. Preparation of tangential sections

On the reconditioning day, all the animals were sacrificed at 30 min after the foot-shock and the hippocampus was dissected and placed in cooled phosphate-buffered saline (PBS). Whatman 3 mm paper (Maidstone, England) wetted with PBS was placed on a flat cellulose acetate filter of a vacuum filtration system (pore diameter, 0.45 μm, Corning Inc., NY, USA). Aluminum foil was extensively perforated and put on the 3 mm paper. Each dissected hippocampus was put on the flat aluminum foil with the pyramidal cell layer of the CA1 and subiculum closest to the foil. The hippocampus was covered with polyvinylidene film and the vacuum was applied, which flattened the spherical pyramidal cell layer. The flattened hippocampus was embedded in Tissue-Tek OCT compound and immediately frozen on dry ice powder (tangential block). Needle holes were punched in the tangential block as location markers and the block was then sliced in parallel with the flatten pyramidal cell layer to make serial sections (tangential sections, 10 μm thick). Approximately 20–30 serial sections containing the whole pyramidal cell layer were used for the reconstruction.

2.3. In situ hybridization

A part of the *Arc* cDNA (nucleotides 760–1380, where the adenine residue of the initiation codon is designated 1) was amplified by PCR and subcloned into the pCRII-TOPO vector (Invitrogen Corp., Carlsbad, CA, USA) to generate pCRII-situ. pCRII-situ was digested with BamHI or EcoRV

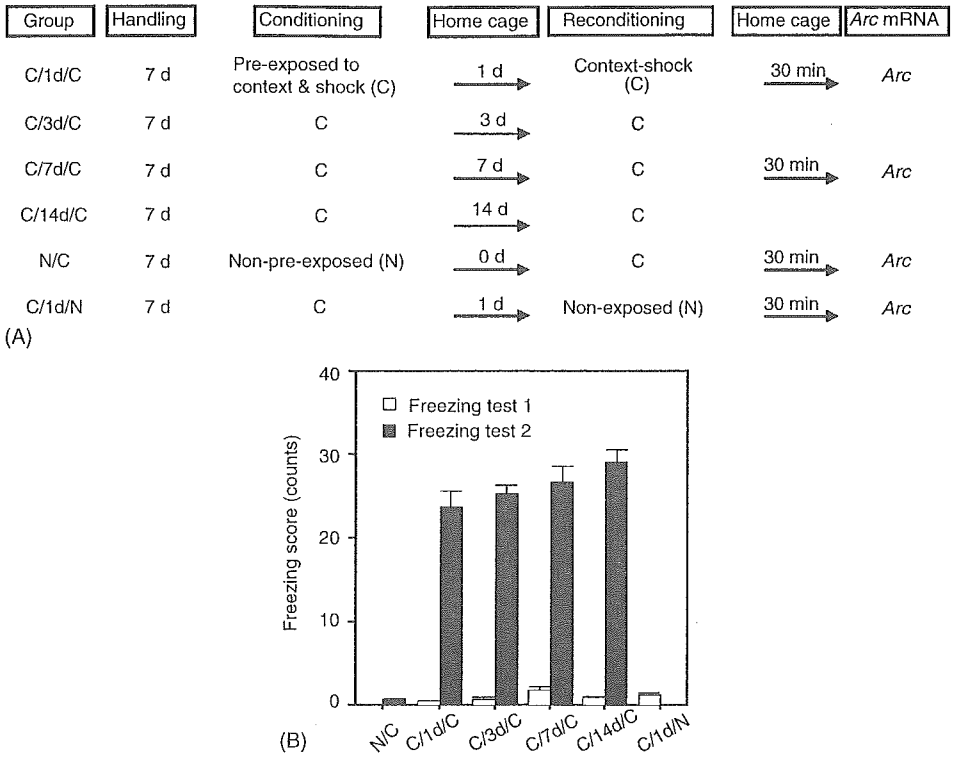

Fig. 1. Contextual fear-conditioning task. (A) Experimental design of contextual fear conditioning. (B) Freezing responses during the first 5 min of the conditioning session (freezing test 1, white bar) and during the first 5 min of reconditioning session (freezing test 2, black bar) (number of animals = 6 for each condition).

to generate templates for in vitro transcription of antisense or sense probes, respectively. Digoxigenin (DIG)-labeled antisense and sense cRNA probes were produced by transcription with T7 and Sp6 RNA polymerases, respectively.

Tangential sections were fixed in 4% formaldehyde in PBS, pH 7.0, for 30 min, treated with 0.3% Triton X-100 in PBS, followed by incubation in 0.2N HCl for 20 min. The sections were then post-fixed with 4% formaldehyde in PBS for 10 min, and treated with 0.2% glycine in PBS for 15 min. Hybridization was performed at 42 °C, overnight, in hybridization buffer (50% formamide; 20 mM Tris–HCl, pH 8.0; 2.5 mM EDTA, pH 8.0; 300 mM NaCl; 0.25% SDS; 10% dextran sulfate; 100 mg/mL of yeast tRNA (Sigma, St. Louis, MO, USA)). Sections were washed for 1 h at 42 °C with 50% formamide in 2× SSC (0.3 M NaCl, 30 mM sodium citrate, pH 7.0), and then washed twice with solution B (10 mM Tris–HCl, pH 8.0, 500 mM NaCl) at room temperature for 15 min. Sections were treated with RNase A (20 μg/mL in solution B) at 37 °C for 30 min, followed by washes with 50% formamide in 1× SSC and then with 50% formamide in 0.5× SSC for 1 h at 42 °C. After equilibration with maleate buffer (0.1 M maleic acid, 0.15 M NaCl, pH 7.5) for 1 h, sections were treated with 10% blocking reagent (Roche Diagnostics, Basel, Switzerland) in maleic acid buffer. Sections were incubated overnight at 4 °C with 1:1000 diluted alkaline phosphatase-conjugated anti-DIG antibody (Roche Diagnostics), washed with maleate buffer, and then equilibrated with reaction buffer (100 mM Tris–HCl, pH 9.0; 100 mM NaCl; 50 mM $MgCl_2$). Transcripts were detected with 5-bromo-4-indolyl phosphate *p*-toluidine salt and 4-nitro blue tetrazolium chloride (NBT) in the reaction buffer at 4 °C for 120 h. After recording images of the *Arc* signal, the sections were de-stained with ethanol (95%), overnight, and then re-stained with Nissl.

2.4. Reconstruction of a two-dimensional flat map

Images of *Arc* signals and Nissl-staining were acquired from sections using a 4× objective lens and a cooled CCD camera (Hamamatsu Photonics, Shizuoka, Japan) with an OptiScan Motorized Microscope Stage System (Meyer Instruments Inc., Houston, TX, USA). Acquired images were analyzed using Image Pro Express (Media Cybernetics, Silver Spring, MD, USA), Meta Morph (Universal Imaging Corporation, Downingtown, PA, USA), and Photoshop software (Adobe, San Jose, CA, USA).

Each image of a Nissl-stained serial section was handled as a layer and stacked using the Image Pro Express software. The configuration of each image was adjusted based on the positions of the marker holes (black dots in Fig. 3A) and blood vessels spanning adjacent sections. Each image of the *Arc* signal was then stacked by the same method. Background was subtracted from each *Arc* image in which the background value of each section was defined as the averaged value of four independent areas (100 × 100 pixels)

of the fiber bundle nearby CA3 (Fig. 3C, asterisk), which showed no detectable *Arc* signal.

2.5. Quantitative and statistical analyses

The *Arc* signals were binarized with appropriate threshold values so that the *Arc*-positive pixels occupied 0.5% of the total pixels in the assessed area (corresponding to the subiculum, CA1, and CA3 surrounded by the broken line in Fig. 3D) of the merged image. To display the *Arc* signal distribution in the two-dimensional map (see Fig. 4), the assessed area were divided into small areas of 20 × 20 pixels (1 pixel corresponds to 2.5 μm). The number of Arc-positive pixels was counted for each small area. Pseudo-colors, purple, blue or yellow, were assigned to each small area when it contained 1–3, 4–7 or >8 *Arc*-positive pixels, respectively. To analyze the relative *Arc* expression profile along the hippocampal longitudinal axis (see Fig. 5), the merged image was divided into 100 areas along its axis. The number of the binarized *Arc*-positive pixels in each area was counted.

Analysis of statistical significance between groups were conducted by two-way ANOVA and assessed by Fisher's PLSD.

3. Results

3.1. Behavioral paradigm

To clarify temporal changes in neural activity of the hippocampus following initial learning, we modified the paradigm of classical contextual fear conditioning (Fig. 1A). All the rats were habituated to handling for seven consecutive days. The first group of rats (C/1d/C, C/3d/C, C/7d/C, and C/14d/C) were pre-exposed to context (conditioning chamber) and shock (C) on the conditioning day. After a delay interval in their home cages of 1, 3, 7 or 14 days, the rats were again exposed to context, and freezing behavior was observed. For C/1d/C and C/7d/C, rats received an additional shock exposure immediately after the freezing test (reconditioning). In the second group, non-pre-exposed group (N/C), rats were exposed to context and freezing behavior was monitored for 5 min. The rats were then exposed to shock. The third group of rats (C/1d/N) were pre-exposed to context and shock (C), and left in their home cage for 1 day.

All the animals showed enhanced freezing behavior when they were exposed to context at various intervals after the conditioning (Fig. 1B), indicating that fear-conditioned memory was preserved over 14 days under our experimental conditions.

For *Arc* analyses, rats were sacrificed 30 min after the reconditioning session for the first two groups and after the 1 day delay in their home cage for the third group, and *Arc* mRNA expression was analyzed by in situ hybridization. Thus, all the groups of rats except the third group were exposed to context and shock 30 min prior to analyzing *Arc* mRNA expression. Differences among these animals were either an interval between conditioning and reconditioning or an experience of conditioning (Fig. 1A).

3.2. Arc mRNA expression following contextual fear conditioning

Induction of *Arc* mRNA in the hippocampal CA1 region has been linked to neural information processing (Guzowski et al., 1999; Guzowski et al., 2001; Kelly and Deadwyler, 2003). We, therefore, chose *Arc* gene expression as an indicator of neural activity that represents information processing during memory formation, consolidation, and retrieval.

Contextual fear conditioning requires the hippocampus for acquisition, storage, and retrieval of fear memory. As expected, the *Arc* mRNA signal increased in a subpopulation of neurons in the CA1 region and the subiculum 30 min after conditioning (N/C group) (Fig. 2). A similar increase in the

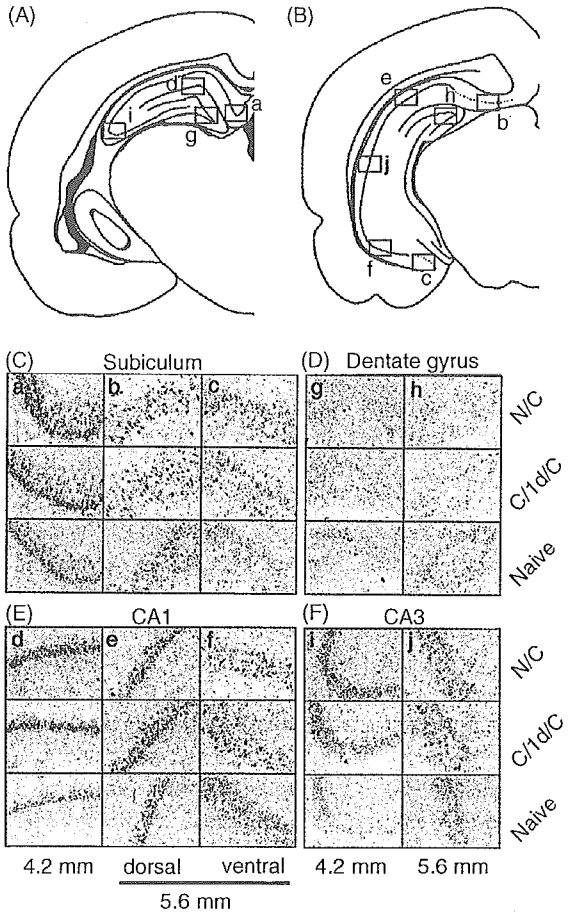

Fig. 2. Expression of *Arc* mRNA following contextual fear conditioning. (A and B) Schematic representations of coronal section at 4.2 mm (A) and 5.6 mm (B) posterior to bregma. Red squires indicate a location of pictures in (C–F). Coronal sections at 4.2 and 5.6 mm posterior to bregma were hybridized with the *Arc* cRNA probe. (C) Subiculum, (D) dentate gyrus, (E) CA1, and (F) CA3. Note that the coronal sections at 5.6 mm contain both dorsal and ventral areas of the CA1 and subiculum.